

# Distributed Space Systems

Simone D'Amico, PhD.

*Space Rendezvous Laboratory ~ Stanford University*

## Solutions to proposed problems

Sebastián E. García

Electronics development ~ sebastian at slabs dot com dot ar

13<sup>th</sup> december, 2015

## Problems set 1

### 1.1.a DSS main application areas

The main applications of **DSS**, are: Planetary Science, Space Science and Technology Improvement.

On the Planetary Science area, we note that constellations (loose formations) of traditional spacecraft (**S/C**) for Earth remote sensing are already here (e.g., the Morning Constellation which included **CoNAE**'s **SAC-C** satellite) though they (at most) have very low interaction within **S/C** vehicles. We are currently seeing private efforts (e.g., Planet Labs, Satellogic) to build constellations of low-cost – non-traditional development cycle – nano-satellites for electro-optic Earth imaging. In the near future, we could expect breakthroughs in the following Formation Flying (**FF**) applications: **SAR** interferometers (**LEO**) delivering highly accurate **DEM** models; gravimeters (**LEO**) delivering highly accurate Earth's gravity models on a global scale.

Regarding Space Science, there's expectation on electro-optical technologies deployed in **FF**, such as dual **S/C** telescopes (**HEO**) achieving large focal lengths, and multi-**S/C** telescopes (**HEO**) with active-controlled mirrors.

Promising applications for **S/C** technology improvement on rendezvous and docking seems to be: debris removal and on-orbit **S/C** servicing. This will likely happen in the mid-term, though.

---

### 1.1.b DSS main mission architectures

Three main architectures of **DSS**, are (in order of decreasing control accuracy and increasing inter-satellite distance): **S/C** rendezvous and docking, **S/C** **FF**, and **S/C** constellation.

---

### 1.1.c Differences between historic, contemporary and future DSS

The **DSS** historically achieved milestones are very important and provide many lessons, though were focused on short-time events with ground control, supported with high (cold war) budgets.

Currently, there is an effort to develop this area, for long duration events managed autonomously by the **S/Cs**, although space agencies have typically very tight budgets for this kind of projects.

For the future, it is expected to expand the current achievements with more distributed and more miniaturized systems, as well as systems/subsystems standardization allowing for lower implementation costs and more responsive (e.g., to emergencies/catastrophes) space missions.

---

### 1.1.d DSS: Past and upcoming missions

Examples of past **DSS** missions:

- **DLR's TanDEM-X/TerraSAR-X**. Main objective: Generate global accurate **DEMs** from **SAR** interferometry obtained with radars onboard two **S/Cs** operating in **FF** architecture.

- **DLR's PRISMA**. Main objective: FF technology demonstration mission, using different relative navigation schemes: GNSS-based, RF-based, and vision-based techniques.

Examples of upcoming DSS missions:

- **NASA-ESA's LISA**. Main objective: Detect gravitational-wave induced strains in space-time by measuring changes of the separation between fiducial masses in three S/C  $5Mkm$  apart (high-distance/high-accuracy application).
  - **NASA's NWO**. Main objective: Discover and directly image Earth-like planets using a combination of a starshade S/C and telescope S/C, separated at a distance of  $50Kkm$ .
- 

### 1.1.e DSS: Fuel-use drivers

The typical fuel-use drivers, are:

- Mission requirements (including “absolute” operating conditions, e.g., required formation altitude);
  - initial conditions;
  - navigation uncertainties;
  - dynamical process noise;
  - actuation errors;
  - algorithms (its correctness, and how well is exploited the available information in the particular application environment).
- 

### 1.1.f Formation control strategies

There are many formation control strategies proposed in the literature. E.g.:

- LQR;
  - MPC;
  - Lyapunov.
- 

### 1.1.g Practical formation control strategy

The most common formation control strategy seems to be Schaub-Alfriend's “4 impulses” method, and similar ones exploiting the inversion of the state transition matrix. The main reasons are:

- mission heritage (well known, proven and ready technology);
  - simplicity;
  - determinism;
  - impulsive nature;
  - propellant economy.
-

### 1.1.h PRISMA mission relative navigation

The relative navigation approaches adopted in the PRISMA technology demonstration mission, are:

- Based on GNSS,
  - cooperative, relying on GNSS constellation,
  - phase difference = projected baseline + bias,
  - ambiguity resolution;
- Based on Radio Frequency,
  - cooperative, self-contained,
  - pseudolites providing GPS-like signals,
  - applicable for deep space navigation;
- Vision-based,
  - (non-)cooperative, optical/infrared,
  - high dynamics range: far- to short-range,
  - support angles-only to full pose estimation.

---

### 1.2.a Coordinate systems

- Earth-Centered Inertial (ECI) CRD coordinate system:
  - fundamental plane: Earth's equatorial plane,
  - origin: Earth's CM,
  - axes pointing:  $\hat{x}$  : vernal equinox,  $\hat{z}$  : Earth's north pole,  $\hat{y}$  : completes the triad;
- Earth-Centered, Earth-Fixed (ECEF) CRD non-inertial (rotating) coordinate system:
  - fundamental plane: Earth's equator,
  - origin: Earth's CM,
  - axes pointing:  $\hat{x}$  : Earth's 0° latitude (Equator) and 0° longitude (Greenwich),  $\hat{z}$  : Earth's north pole,  $\hat{y}$  : completes the triad;
- Perifocal CRD inertial (without perturbations) coordinate system:
  - fundamental plane: instantaneous orbital plane,
  - origin: primary body's CM,
  - axes pointing:  $\hat{x}$  : orbital periapsis,  $\hat{z}$  : orbital's angular momentum,  $\hat{y}$  : completes the triad;
- RTN (LVLH or Hill's frame) CRD non-inertial (rotating) coordinate system:
  - fundamental plane: instantaneous orbital plane,
  - origin: S/C's CM,
  - axes pointing:  $\hat{x} (\hat{r})$  : ("radial") position vector,  $\hat{z} (\hat{n})$  : ("normal") orbital's angular momentum,  $\hat{y} (\hat{t})$  : completes the triad; in case of a circular orbit the  $\hat{t}$  versor will be tangential to the orbit (i.e., parallel to the velocity vector);
- Polar non-inertial (rotating) coordinate system:
  - fundamental plane: instantaneous orbital plane,
  - origin: primary body's CM,
  - axes pointing:  $\hat{r}$  : ("radial") position vector,  $\hat{\theta}$  : counter-clockwise (as seen from the orbital's angular momentum vector's "tip") from some reference line (e.g., line of nodes);

### 1.2.b Restricted two-body problem assumptions

The assumptions are:

- only gravity force acting on orbiting body, due to the (Newton's) attraction of the primary body, no other external/internal forces;
- both bodies have spherical shape;
- primary body's mass is much larger than orbiting body's mass.

### 1.2.c Fundamental orbital differential equations: solution in polar coordinates

The fundamental orbital (vectorial, nonlinear, time-varying) differential equation (d.e.) for the restricted two-body problem, is:

$$\ddot{\mathbf{r}} + \frac{\mu\mathbf{r}}{r^3} = \mathbf{0}$$

Expressing this d.e. in polar coordinates, integrating, taking account for the constants of motion (total specific energy  $\varepsilon$  and specific angular momentum  $\mathbf{h} = \mathbf{r} \times \mathbf{v}$ ), and with some manipulation, we obtain a single, first order d.e. on  $\frac{dr}{d\theta}$ . Its solution in polar coordinates, with initial condition  $\theta_0 = \omega$  (argument of perigee), is a conic section,

$$r = \frac{p}{1 + e \cos f}$$

, with eccentricity  $e = \sqrt{1 + 2\varepsilon h^2/\mu^2}$ , semilatus rectum  $p = h^2/\mu$ , and true anomaly  $f = \theta - \omega$ .

### 1.2.d Solution of the orbital differential equations in inertial coordinates

The following are the steps required to derive the solution of the orbital d.e. in inertial ECI coordinates, in terms of the classical orbital elements and time.

1. Starting point: the solution of the fundamental d.e. in polar coordinates (cone section equation): radius vector as a function of the true anomaly  $f$ .
2. Considering elliptic orbits<sup>†</sup>, we perform a geometric construction of a "boundary circle" and its auxiliary parameter *eccentric anomaly*  $E$ , which is (geometrically) related to the true anomaly  $f$ . On the auxiliary circle, a corresponding "virtual point" is moving with angular position  $M$  (mean anomaly) and with constant angular velocity, the mean (angular) motion  $n = \sqrt{\mu/a^3}$ . Since  $M$  provides a link between time  $t$  (through constant  $n$ ) and the eccentric anomaly  $E$  (through Kepler's equation), we finally found a mapping between  $f$  and  $t$ ; i.e.:  $t \leftrightarrow M \leftrightarrow E \leftrightarrow f$ . Now,  $f$  is a function of  $a, e, t$  and  $M_0$  (mean anomaly at epoch). Considering also the (constant) eccentricity vector  $e$ , the equations of motion could be integrated using these constants.
3. We write the position vector in the perifocal coordinate system,  $[\mathbf{r}]_{\mathcal{P}}$  (an inertial frame for this restricted 2-body problem), in terms of  $r$  and  $f$ . We write the velocity vector in the perifocal coordinate system,  $[\mathbf{v}]_{\mathcal{P}} = [\dot{\mathbf{r}}]_{\mathcal{P}} = \left[ \frac{d\mathbf{r}}{df} \right]_{\mathcal{P}} \dot{f}$ , where the first term is directly obtained from  $[\mathbf{r}]_{\mathcal{P}}$ , and the time derivative of the true anomaly is obtained from the specific angular momentum:

$$\mathbf{h} = h\hat{\mathbf{z}} = r^2\dot{\theta}\hat{\mathbf{z}} \Rightarrow \dot{f} = \dot{\theta} = \frac{h}{r^2}$$

In all cases, we replace  $r$  with the polar solution (conic equation), based on the orbital/geometric parameters.

4. The next step is to build the rotation (DCM) matrix between  $\mathcal{P}$  and  $\mathcal{I}$  (ECI) frames:  $T_{\mathcal{P}}^{\mathcal{I}}$ . This could be done composing three elementary clockwise rotations by the Euler angles (1-3-1 sequence): rotate an angle  $\omega$  (argument of perigee) around  $\hat{\mathbf{h}}$  (angular momentum), rotate an angle  $i$  (inclination) around  $\hat{\mathbf{l}}$  (line of nodes), rotate an angle  $\Omega$  (right ascension of the ascending node) around  $\hat{\mathbf{z}}$  (primary body's rotation axis).

<sup>†</sup> A direct integration of the law of areas relating time and angular position in orbit doesn't result in a useful  $f \leftrightarrow t$  relation, except for circles/parabolas.

5. Finally, we apply the rotation to obtain:

$$\begin{aligned}\mathbf{r} &= T_{\mathcal{P}}^T(\omega, i, \Omega)[\mathbf{r}]_{\mathcal{P}}(a, e, M_0, t) = \mathbf{r}(a, e, i, \Omega, \omega, M_0, t) \\ \mathbf{v} &= \dot{\mathbf{r}} = T_{\mathcal{P}}^T(\omega, i, \Omega)[\dot{\mathbf{r}}]_{\mathcal{P}}(a, e, M_0, t) = \mathbf{v}(a, e, i, \Omega, \omega, M_0, t)\end{aligned}$$


---

### 1.2.e Solution of the orbital differential equations with time as independent variable

In the previous answer we included the steps necessary to derive the solution of the orbital d.e. with time as independent variable, using the mapping:  $t \leftrightarrow M \leftrightarrow E \leftrightarrow f$ .

That is, using  $f = f(a, e, M_0, t)$  in the inertial (ECI) solutions of  $\mathbf{r}$  and  $\mathbf{v}$ , we end up with a final expression in terms of the six classical orbital parameters  $\mathfrak{oe} = \{a, e, i, \Omega, \omega, M_0\}$ , while the time  $t$  is considered the independent variable.

---

### 1.2.f Conservation of orbital elements

In the restricted two-body problem *all* orbital elements are conserved.

---

### 1.2.g Other quantities conserved in the restricted two-body problem

Key quantities conserved in the restricted two-body problem, are: (specific) angular momentum  $h$  and total energy  $\varepsilon$ . Also, the eccentricity vector (Laplace-Runge-Lenz)  $e$  is conserved due to the conservative vector field.

---

### 1.2.h Keplerian orbit elements degeneration

The Keplerian orbit elements can become degenerate; e.g., circular orbit case (no unique line of apsides then  $\omega$  and  $f$  are undefined), equatorial orbit case (no unique line of nodes, then  $\Omega$  undefined).

To circumvent this problem we can define alternative orbital elements. However, we keep in mind that we are looking for the simplest representation that is nonsingular to our particular application case.

Replacing  $\{e, M, \omega\}$  by  $\{q_1 = e \cos \omega, q_2 = e \sin \omega, \lambda = \omega + M\}$  works well, except for equatorial orbits where  $\{a, q_1, q_2, i, \Omega, \lambda\}$  is still singular. If the application case requires the removal of all the singularities of the classical orbital elements, *equinoctial elements* could be used, or another representation that avoids the Euler angles (in the perifocal to ECI transformation), using instead a quaternion parameterization.

---

### 1.2.i Orbit characteristics from “frozen” position and velocity vectors

We assume that the restricted two-body problem hypotheses (approximately) hold, and that the provided position and velocity corresponds to a same instant of time. Assume that the time unit  $TU_E$  is defined such that the speed of the orbiting body in a hypothetical circular reference orbit at  $1DU_E$  (just above the planet) is  $1DU_E/TU_E$ . Then, the gravitational parameter value is  $\mu_{UE} = 1DU_E^3/TU_E^2$ .

Since the inertial velocity vector has no component in the  $\hat{k}$  axis, and due to conservation of angular momentum, the movement is restricted to the equatorial plane (defined by versors  $\hat{i}, \hat{j}$ ). Also, since the velocity vector is not perpendicular to the position vector, we note that the orbit is not circular ( $e \neq 0$ ).

Computing the total specific energy,

$$\varepsilon = \frac{v^2}{2} - \frac{\mu_{UE}}{r} = \frac{1}{2} \frac{DU_E^2}{TU_E^2} - \frac{1}{2} \frac{DU_E^2}{TU_E^2} = 0$$

, we see that the orbit is a parabola.

---

## Problems set 2

### 2.1.a Fundamental d.e. in the presence of perturbations

When perturbations act on the body, the motion is no longer Keplerian. The fundamental (nonlinear, vectorial) d.e. obtained by applying Newton's second law of motion, is now non-homogeneous, with a "forcing function" term. This can be solved applying Euler/Lagrange's variation-of-parameters (VOP) method.

### 2.1.b VOP method description

- For example, consider a second order d.e., with a "forcing function" (non-homogeneous equation).
- Take the homogeneous ("unperturbed", nominal motion) solution of the d.e..
- Consider the integration constants of the homogeneous solution, as time-dependent.
- Differentiate the homogeneous solution w.r.t. time, and consider the integration constants and their derivatives as our new "state variables".
- Doing so, now we have more degrees of freedom, then we equate the last expression to an ad-hoc constraint  $\Xi(t)$ .
- Solve (differentiate again, replace in d.e.) for the solution in terms of the new, time-dependent parameters.
- The  $\Xi(t)$  term will cancel out in the process (*symmetry property*).

### 2.1.c LPE and GVE equations

We consider now the modified scenario (w.r.t. the restricted two-body problem), adding a "forcing function"  $d$  in the fundamental d.e., that represents "perturbing" specific forces applied to the orbiting body. Applying the VOP formalism, now the set of orbital elements (the integration constants) are required to be functions of time,  $\mathbf{oe}(t)$ , so:

$$\mathbf{r} = \mathbf{F}[\mathbf{oe}(t), t] \Rightarrow \dot{\mathbf{r}} = \frac{\partial \mathbf{F}}{\partial t} + \frac{\partial \mathbf{F}}{\partial \mathbf{oe}} \dot{\mathbf{oe}}$$

In the process it is needed to impose a constraint; it is typically chosen the so called *osculation constraint*:

$$\frac{\partial \mathbf{F}}{\partial \mathbf{oe}} \dot{\mathbf{oe}} = \mathbf{0}$$

This constraint gives rise to the concept of *osculating orbit* and its corresponding *osculating orbital elements*.

We have, according to the nature of the forcing function:

- **Lagrange's Planetary Equations (LPE):** The d.e. describing the temporal change of the Orbital Elements (OE) within a conservative vector field (in the presence of a position-only dependent perturbing potential function).
- **Gauss' Variational Equations (GVE):** They model the time evolution of the OE due to an *arbitrary* (completely general) perturbing specific force (or control input), resolved in the S/C's own RTN frame.

### 2.1.d Incorporation of perturbations

We can incorporate perturbing gravitational effects (conservative field), by considering the dominant coefficients (e.g.,  $J_2$  zonal harmonics) in the series representation of the geopotential, obtaining its spatial gradient, and plugging it as the perturbation specific force term in the LPE solution of the fundamental d.e..

As the GVE admits any arbitrary perturbation force, we can use them with the gradient of a geopotential (conservative field), atmospheric drag forces (non-conservative) and also with impulsive maneuvers (non-conservative).

### 2.1.e Key effects of $J_2$ , drag, and impulsive maneuvers

The key effects of  $J_2$ , drag, and impulsive maneuvers on an (e.g., elliptic case) orbit solution, are:

- **$J_2$  (in mean terms):** .
  - Mean OE  $\{\bar{a}, \bar{e}, \bar{i}\}$  are unaffected.
  - There are secular growths on  $\{\omega, \Omega, M_0\}$ .
- **Atmospheric drag:**
  - The orbit decays: secular variation on  $a \downarrow, \varepsilon \downarrow$  (remember  $\varepsilon < 0$ ).
  - The orbit becomes gradually circular<sup>†</sup>: secular component variation on  $e \downarrow$ .
  - There are periodic variations on  $\{e, \omega, M\}$ .
  - The orbit orientation is unaffected:  $i$  and  $\Omega$  are held constants.
- **Impulsive maneuvers:** Under the *impulsive thrust assumption*, we can analyze the effects of maneuvers on the set of OE, replacing in the GVE the perturbation components along each axis (RTN frame) by the variations of velocity due to corresponding impulses, replacing time derivatives of OE by its net variation, and taking account (when the approximation is appropriate on a given time interval) for average values in the expressions. E.g.: calculating  $\Delta v$  needed for certain  $\Delta$ OE compensation due to an undesired secular effect (accumulated in some time interval), in order to maintain a desired orbit.

### 2.1.f Inclinations which remove secular ( $J_2$ ) effects on the orbit elements

Should we have a computing system with infinite precision (no numerical errors), we could achieve:

- Choosing  $\bar{i} = \pi/2$  removes secular growth on  $\bar{\Omega}$ .
- Choosing  $\bar{i} = \arccos(\sqrt{1/5})$  removes secular growth on  $\bar{\omega}$ .
- Choosing  $\bar{i} = \arccos(\sqrt{1/3})$  removes secular growth on  $\bar{M}_0$ .

### 2.1.g Secular effects of atmospheric drag on the orbit elements

This was answered in question §2.1.e.

### 2.1.h Out-of-plane impulsive maneuvers

Out-of-plane impulsive maneuvers do affect the in-plane orbit motion, since the GVE's equation for the time evolution of the argument of perigee  $\omega$  (an in-plane OE) has a term including the cross-track (out-of-plane) perturbation component  $d_h$ .

Now, if we describe the phasing of the S/C along its orbit using the so-called longitude

$$\lambda = \omega + M_0 + \Omega \cos i$$

<sup>†</sup> We would need to use a set of nonsingular OE to avoid the singularity at a circular orbit presented by the classical set of OE.

, then after math manipulation we find that the effect of the out-of-plane maneuver is cancelled, and the time evolution of  $\lambda$  is governed by the following d.e.:

$$\frac{d\lambda}{dt} = -\frac{\Omega}{h}$$

, where we have omitted terms including in-plane components of the maneuver, for simplicity.

### 2.1.i Maneuver placement

Looking at the GVE equations, we note:

- **Change inclination only:** Maneuver completely oriented (RTN) in cross-track direction  $d_h$ , applied at one of the nodes ( $\theta = 0$  or  $\theta = \pi$ ).
- **Change right ascension of ascending node only:** Maneuver completely oriented (RTN) in cross-track direction  $d_h$ , applied at  $\theta = \pi/2$  or  $\theta = 3\pi/2$ . As considered in §2.1.h, the phasing of the S/C along its orbit will need to be described using the longitude  $\lambda$  (instead of  $\omega$ ).
- **Change semimajor axis:** In RTN frame, the maneuver must be oriented in radial  $d_r$  and/or along-track  $d_\theta$  direction. In NVH frame, the maneuver must be oriented in the velocity vector  $d_v$  direction.

### 2.2.a Numerical simulation of the relative motion

Two ways to simulate numerically the relative motion between FF S/Cs, including perturbations, are:

- **“True motion” simulation.** An accurate (high computing power required) numerical integration of the nonlinear d.e. of motion (i.e. Newton’s second law including considered perturbations) corresponding to each S/C (perturbed two-body orbiting Earth), each one with its corresponding initial conditions. We obtain, for each vehicle, its position and velocity in ECI frame coordinates, from which we compute the relative position and velocity vectors between S/Cs. In this way, we can accurately capture geopotential effects up to  $J_6$  if required. After the algorithm is validated, this will be the “golden”, “true” solution to be used as a reference for comparisons to other simulation (or onboard real-time computing) schemes.
- **GVE-based simulation.** Involves the integration of the GVE d.e. (including considered perturbations) for each S/C, each one with its corresponding initial conditions. We obtain, for each S/C, the time evolution of its osculating OE set, which could be translated (using the appropriate mapping function) to the vehicle’s inertial position and velocity, and then compute the relative position and velocity between S/Cs.  
*NOTE: Due to the position of this question in the list, I understand that it is not asking about OE differences or ROE set.*

### 2.2.b Computing relative position and velocity in RTN frame

We assume have integrated the nonlinear equations of motion for each S/C vehicle, obtaining position  $r$  and velocity  $v$ , and computed the relative values between S/C:  $\delta r$  and  $\delta v$ . All these are expressed in ECI frame.

Two ways to compute the relative position and velocity of FF S/Cs in the chief’s RTN frame, are:

- **Projection/differentiation method.** We can orthogonally project  $\delta r$  along each of the chief’s RTN frame axis directions, obtaining the components of the relative position on the radial, along-track and cross-track directions. Then we can differentiate each component w.r.t. time, obtaining the relative velocity vector expressed in chief’s RTN frame.  
*NOTE: As two projections require the use of the angular momentum vector, we note that the resulting velocity component expressions require the knowlegde of the inertial acceleration of the chief:  $\dot{v}_0(t)$ .*

- **Rotation method.** We build the rotation DCM “ $T$ ” between frames, and apply it to translate:

$$[\delta \mathbf{r}]_{RTN} = T \delta \mathbf{r} ; [\delta \mathbf{v}]_{RTN} = T \delta \mathbf{v} .$$

One possible way to build the DCM is placing in each of its columns the ECI coordinates of the base vectors of the RTN system:  $T(\Omega, i, \theta) = \begin{bmatrix} \hat{\mathbf{R}}_{ECI} & \hat{\mathbf{T}}_{ECI} & \hat{\mathbf{N}}_{ECI} \end{bmatrix}$

### 2.2.c Mean and osculating orbit elements

The *osculating orbit* is the two-body trajectory that would be followed after time  $t$ , if at that instant the perturbing specific force  $d$  were to suddenly vanish, thereby making valid the homogeneous fundamental d.e.. The orbital elements that satisfy the Lagrange constraint are called *osculating orbital elements*.

Applying the averaging theorem to our fundamental d.e., we obtain expressions of (simpler) differential equations characterizing the time evolution of the *mean orbital elements*.

The solution of the equations of motion in terms of a mean OE state captures secular effects. These are the effects that we care about when developing FF applications.

To convert from osculating to mean orbital elements is not difficult as it requires taking time averages, but the inverse mapping is more involved. Two possible methods, are:

- **Algorithm based on Bower’s theory.** It is a first order approximation, including  $J_2$  effects, appropriate for computing onboard S/C. This algorithm produces a one-to-one mapping, with the simplicity of just requiring to change the sign of the  $J_2$  coefficient to go back and forth between sets of osculating and mean OE.
- **Iterative algorithm.** Based on the Jacobian matrix for the transformation between mean and osculating OE. This is more accurate than the former method, requires more computing power and can be used for simulations on ground.

### 2.2.d Nonlinear equations of relative motion: assumptions

The assumptions behind the nonlinear equations of relative motion are the same as in the two-body problem of absolute motion. Besides this generality, later we will want to restrict to the case of elliptic orbit for the chief, and apply the energy matching condition between chief and deputy, in order to ensure bonded relative orbits.

In the set of three scalar expressions obtained for the nonlinear equations of relative motion, the whole right hand side are the applied forces, while the whole left hand side are the relative acceleration components measured (time derivatives taken) in the ECI frame and expressed as coordinates of the RTN frame. The scalar derivatives  $\{\dot{x}, \dot{y}, \ddot{x}, \ddot{y}, \ddot{z}\}$  appearing *inside* each left hand side expression, are time derivatives taken in the RTN frame, and expressed in the same RTN frame.

### 2.2.e Nonlinear equations of relative motion: closed-form solution, equilibria

The nonlinear equations of relative motion admit a closed-form solution in the OE state space, but not in cartesian state space.

For the case of non-constant chief’s angular velocity, the general non-perturbed equations admit a trivial relative equilibrium point at  $x = y = z = 0$ ; i.e., the deputy will appear stationary in the chief’s RTN frame if and only if their positions coincide (non practical...).

### 2.2.f Commensurability

If the two involved S/C vehicles follow Keplerian elliptic orbits and their periods are restricted to be m:n commensurable (the ratio of the periods is a rational number), the resultant relative motion will be periodic. This guarantees “local” boundness (short scale term) of the relative motion. Due to the dependence of the orbital period with total specific energy, and thus with semimajor axis, the commensurability condition on  $T_1/T_2$  also implies constraints on  $\varepsilon_2/\varepsilon_1$  and  $a_1/a_2$  (not rational in general, though).

In formation-flying applications, it is convenient to apply a 1:1 condition, where total energies and semimajor axes match.

Applying the Coriolis theorem to derive the deputy planar kinematics in RTN frame “as seen” from the inertial frame, and applying the total energy matching condition, we obtain a constraint over the initial conditions of the equations of relative motion, that guarantees bounded relative orbits.

### 2.2.g Simplifications of relative motion with circular reference orbit

We can simplify the equations of relative motion, imposing the condition of the chief S/C moving in a circular orbit:  $\dot{\theta}_0 = n_0 = \text{constant}$ ,  $\ddot{\theta}_0 = 0$ , and  $r_0 = a_0 = \text{constant}$ . Replacing this in the original d.e. system, the resulting d.e. system is autonomous (time-invariant), though it is still nonlinear, second order and includes coupling between in-plane (radial and along-track axes) and out-of-plane (cross-track axis) motion.

Imposing in the simplified equations the equilibrium condition  $\dot{x} = \dot{y} = \dot{z} = 0$ , the solution for the relative position expressed in the RTN frame is the equation of a circle that coincides with the chief's orbit. That is, it allows for an equilibria continuum: the deputy S/C will appear stationary seen from the chief's RTN frame, if the former is co-located on the circular orbit of the latter.

This equilibrium condition is consistent with the energy matching condition, as the semimajor axes of chief and deputy coincides.

*Libration* is the periodic motion around an equilibrium, arising from small perturbations.

### 2.2.h Hill-Clohessy-Wiltshire (HCW): Linear equations of relative motion

#### 2.2.h.1 Assumptions, derivation, key simplifications, decoupled motions

We can simplify the equations of relative motion, when considering a chief circular orbit and small separations of the co-orbiting spacecraft, as compared with the orbit radius. This can be done applying a first-order Taylor approximation, about the origin of the chief-fixed RTN frame. The obtained equations are much more simple: it is a set of linear, time-invariant d.e., where the out-of-plane motion ( $z$ ) has been decoupled from the in-plane motion ( $x, y$ ).

The linearization process (closeness hypothesis) brings the mentioned motion decoupling. Actually, real applications in FF have shown that this decoupling results an over-simplification of the physical behaviour, not capturing important nonlinear effects as soon as we slightly move from the closeness hypothesis (relative orbit dimension not very small compared to the chief orbit radius).

#### 2.2.h.2 Equilibria, consistency with previous findings, energy matching condition

The solution of the HCW equation has multiple equilibria in the points  $\{x = 0, y = \text{constant}, z = 0\}$ , at first glance an aparent contradiction. This is indeed consistent with the equilibrium condition found in the case of §2.2.g (continuum on the circular chief's orbit), as the coordinate in the along-track axis could be written with a curvilinear coordinate  $y = a\delta\theta$  in the vicinity of the chief-fixed frame, where the Taylor approximation can be considered valid.

The energy matching condition, equivalent to having equal semimajor axis between S/Cs, is a *global* boundedness criterion. Under the validity of the HCW hypotheses, this is *approximately* accomplished when enforcing the *local* boundedness (no relative drift) restriction on the initial conditions (described in the following answers).

## Problems set 3

### 3.1.a HCW equations: characteristics, eigenvalues

Writing the HCW linear system of d.e. in state-space form, we find that the system's matrix has the following eigenvalues:  $\{\pm nj, \pm nj, 0, 0\}$ , showing the presence of periodic oscillation (complex  $\pm nj$  eigenvalues) and secular (zero eigenvalues) modes.

Solving the system, the along-track (chief-centered RTN) component of the relative position exhibits a drift growing linearly with time, i.e. the in-plane motion is unstable, and also an offset term. Additionally, the radial component of the solution has a constant offset term.

The highly underised drift effect can be avoided with a proper selection of the initial conditions; choosing  $\dot{y}(0) = -2nx(0)$ , cancels both the along-track secular drift term and the offset in the radial direction.

Another effect is the uncoupled cross-track component that behaves as an harmonic oscillator. If we want to cancel this, we can do it choosing its initial conditions to be:  $\dot{z}(0) = z(0) = 0$ .

The in-plane components solutions exhibit harmonic terms, all with angular frequency equal to the mean (angular) motion  $n$ .

### 3.1.b HCW equilibria

This question was answered in §2.2.h.

### 3.1.c HCW in amplitude/phase form

Recognizing the harmonic nature of the solutions of the HCW equations, after imposing initial conditions according to the local stability condition  $\dot{y}(0) = -2nx(0)$  (in order to cancel the along-track drift), we can express the solutions in amplitude/phase form: each axis oscillates sinusoidally with angular frequency equal to the mean (angular) motion  $n$ , with given “frozen” (determined by initial conditions) phases and maximum amplitudes. The along-track motion exhibits the previously mentioned bias term, and the coupling between both in-plane coordinates appears as relations on their oscillation amplitudes and phases. The resulting parametric equations represent an elliptic cylinder. Adding a restriction on the phase  $\alpha_x = \alpha_z$  (“phase matching” condition), they become the representation of a 3D ellipse, centered on  $(0, \rho_y, 0)$ .

The RT ( $xy$ ) projection of the relative motion is a parametric representation of a 2:1 ellipse with semimajor axis  $a = 2\rho_x$ , semiminor axis  $b = \rho_x$  and (constant) eccentricity:

$$e = \sqrt{1 - (b/a)^2} = \sqrt{1 - \rho_x^2/4\rho_x^2} = \sqrt{3}/2$$

The RN ( $xz$ ) projection of the relative motion has, in general, an “oval” shape. Imposing the condition  $\alpha_z = \pi/2 + \alpha_x$ , it becomes an ellipse.

### 3.1.d HCW: Difficulty to design bounded relative orbits

In the derivation of the HCW equations, a linearization approximation is performed<sup>†</sup> in the expansion of the differential gravity. However, the initial conditions are also affected.

For example, if chief and deputy S/Cs are required to be in the same circular orbit, after computing the real initial conditions (from a simple geometric construction) and replacing them in the terms of radial offset and along-track drift, both these result non-zero. It can be readily seen that there is in fact a non-zero differential semimajor axis; i.e., the system is not meeting the energy matching condition.

If we run a numerical integration of the nonlinear equations of motion using these initial conditions, the two satellites will drift apart (unbounded relative orbit).

The use of the cartesian coordinate system results in undesirable errors in the solution due to the nonlinear terms. These nonlinear effects can be reduced if a more “natural”, curvilinear coordinate system is used instead. The version of the HCW equations expressed in curvilinear coordinates have essentially the same form (adds no complexity). Now the along-track and cross-track distances are measured along arc lengths (not linear displacements). This reduces the nonlinear effects in the computation of the initial conditions. Note that with the use of the curvilinear coordinate equations we will still have unavoidable errors due to the linearization process, but the errors will be much smaller compared with those implicit in the cartesian expressions.

### 3.1.e Arbitrary eccentricity: Tschauner-Hempel (TH) equations and comparison with HCW

To derive the linearized equations of relative motion for arbitrary eccentricity, we normalize the general nonlinear equations<sup>‡</sup> of relative motion, dividing the relative RTN-frame coordinates by the norm of the chief position vector,  $r_0$ . Furthermore, we express the equations in terms of the true anomaly ( $f$ ) as independent variable.

When the relative position between S/Cs is small compared to the radial distance of the target satellite from the principal body's gravitational center, i.e.  $\|\rho\|/r_0 = \rho/r_0 \ll 1$ , the previously obtained nonlinear dynamic function can be expanded in a Taylor series. The linear form of the equations, neglecting higher-order terms, are known as the Tschauner-Hempel (TH) equations, and have been used extensively to model the rendezvous problem with an eccentric chief orbit. The resultant is a second-order system of LTV d.e. in terms of derivatives of normalized coordinates w.r.t.  $f$ .

<sup>†</sup> Under the assumption of small chief-deputy distance, compared to the chief's orbital radius. <sup>‡</sup> The procedure is valid in presence of a specific force or control law.

The particular case with  $e = 0$  (circular chief orbit) reduces to the **HCW** model. Similarly to **HCW** equations, the linearization has decoupled in-plane and out-of-plane motion. The resultant equations have a similar appearance, but **TH** introduces a new parameter,  $k = 1 + e \cos f$ , that cause the arising of terms with multiplications of sinusoidal factors having the same argument ( $f$ ), thus leading to different effects as described in the following answers.

### 3.1.f Yamanaka-Ankersen (YA) solution to TH equations

#### 3.1.f.1 Solution derivation

An interesting solution to the **TH** equations was provided in the last decade by Yamanaka-Ankersen (**YA**).

In **TH** equations, the decoupled out-of plane normalized coordinate  $\bar{z}$  is a simple harmonic oscillator. We can combine **TH**'s in-plane motion coordinates d.e., to form a single, second-order time-varying d.e. on the normalized radial coordinate  $\bar{x}$ .

**YA** builds on a solution  $\bar{x}_1$  (due to Lawden previous work), from which they obtained a second independent solution  $\bar{x}_2$ , using an identity that relates the integral of a function of  $k(f)$  with  $\mu$ ,  $h$  and  $t$ . With these two independent solutions, they built a third particular solution,  $\bar{x}_3$ . Solving for  $\bar{x}$  enables to obtain  $\bar{y}$  and adding the  $\bar{z}$  solution we have a system of three equations, appearing six integration constants and the integral factor  $I = (\mu^2/h^3)(t - t_0)$ . Eliminating the integration constants and considering  $\bar{x}(t) = [\bar{x} \ \bar{x}' \ \bar{y} \ \bar{y}' \ \bar{z} \ \bar{z}']^T$  as the state vector, we can build the State Transition Matrix (**STM**), which results in a simple form to code in software.

#### 3.1.f.2 Secular effects and its removal

The integral factor  $I$  present in the in-plane motion solutions implies an unbounded oscillation in the radial direction and a linearly-growing drift in the along-track direction. Like the **HCW** approximated restriction on the initial conditions to avoid drift, in the **TH** model we have a similar boundedness condition, that is a better approximation since eccentricity effects are taken into account. This can be done by setting **YA**'s constant  $c_3 = 0$  and solving for relative initial conditions on position and velocity at an arbitrary true anomaly at epoch  $f_0 = f(t_0)$ .

#### 3.1.f.3 Bounded motion condition and comparison to HCW

Except when  $f_0 = 0$  or  $f_0 = \pi$ , the resulting constraint is satisfied for an infinite combination of initial conditions since, for a given initial relative position, it involves initial relative velocities in both radial and along track directions.

Comparing to the **HCW** situation, in the case of **YA** the boundedness condition depends on the true anomaly at epoch,  $f_0$ , and it can be enforced in multiple ways due to the reason commented in the previous paragraph. Besides that in **YA** this condition will be a better approximation (due to the inherent arbitrary eccentricity of the **TH** model), it neither guarantees an absolute bound, since the constraint is still only a first-order Taylor approximation (around chief's vicinity) to the desired  $\delta a = 0$  (energy matching condition).

### 3.1.g TH solution in amplitude/phase form

#### 3.1.g.1 Description and comparison to HCW case

After applying the boundedness condition (derived from  $c_3 = 0$ ) and re-scaling to have dimensional coordinates, the periodic relative position solution of the **TH** equations exhibits in the radial direction (RTN-chief) a standard sinusoidal in true anomaly  $f$  (frozen amplitude and phase), while in the along- and cross-track directions there are combinations of products and divisions of terms having sines and cosines in  $f$ . A Fourier analysis in both cases of the latter two directions (as functions of true anomaly  $f$ ) reveals they have constant terms (biases), a primary harmonic (associated with relative orbit parameters), higher order harmonics (decaying with  $\sim \mathcal{O}(e)$ ), and a phase shift. The appearance of higher-order harmonics in  $y$  and  $z$ , but not in  $x$  coordinate, gives rise to another effect (not present in **HCW**): skewness of the relative orbit plane (i.e., the orbit is no longer planar).

Considering the particular case of a circular chief orbit, the expressions consistently reduce to the **HCW** case when replacing with  $e = 0$  (note that  $nt = f$  in the **HCW** case).

### 3.1.g.2 Achievement of bounded and centered relative motion

The bias in the  $z$  component cannot be controlled because it depends on the relative orbit parameters (determined by the orbit design requirements), while the bias in the  $y$  component (along-track direction) can be removed by an appropriate choice of its parameter  $\rho_y$ . Besides other possible choices, we can apply the so-called amplitude correction  $\rho_y = e\rho_x \cos \alpha_x$ .

---

### 3.1.h HCW and YA: Approximation of differential semimajor axis

Each model's corresponding "zero secular drift condition" is an *approximation* to the desired zero differential semimajor axis condition (energy matching condition).

Given an eccentric chief orbit, the boundness condition obtained for the TH-YA model is a better approximation than that for HCW, since the former model accounts for arbitrary eccentricity. Analogously to the HCW model case, an eventual expression of a solution to the TH equations in terms of curvilinear coordinates is expected to enhance the approximation, due to the nature of the problem's geometry, though I understand this is still under research.

As said, in any case these are approximations due to the inherent linearization process, so in both models we will have  $\delta a \neq 0$ .

---

### 3.2.a Orbital elements differences and relative motion: nonlinear and linear mapping

Using a complete set of Orbital Elements Differences (OED) (invariant under no perturbations) we can avoid to solve a d.e. to obtain the state of the relative motion system. Given  $\delta \mathbf{oe}$  and  $\mathbf{oe}_{chief}$ , the deputy vehicle position (at any time) can be computed by solving Kepler's equation. This framework, without simplification assumptions, gives a nonlinear mapping to obtain the relative position and velocity vectors.

We can obtain a linear mapping between Hill (RTN) coordinates and combinations of OED by assuming  $\rho \ll r_c$ ; that is, a small separation between chief and deputy that implies small angles in the rotation between their RTN frames. This holds for any chief orbit eccentricity and yields a better accurate description of the relative motion compared to the TH-YA approach, because  $\delta a$  is not approximated by the linearization process.

---

### 3.2.b OED description: Choice for the phasing variable

The difference in true anomaly<sup>†</sup>  $\delta f$  is not conserved as a constant quantity, in the condition of general Keplerian orbits restricted with the energy matching condition. It is varying in time.

It can be readily shown that the difference in mean anomaly<sup>‡</sup>  $\delta M$  is invariant in this non-drift condition, so it is a natural selection to describe the relative "phasing" between S/Cs.

---

### 3.2.c OED description: Similarity with the solution of TH equations

The OED space solution is the analog of the TH-YA solution, having the same structural form, now expressing the relative orbit coordinates as combinations of OED.

It is expressed with  $f$  as an independent variable, though  $M_c(t)$  (contained in  $\delta M$ ) arises as another independent variable, in the case of drift ( $\delta a \neq 0$ ). The difference in semimajor axis  $\delta a$  appears explicitly and is also contained in  $\delta M$ ; this is an important contrast when comparing to the TH-YA solution. We have the expected sinusoidal functions terms with period  $2f$  (which in TH-YA are hidden in the products between sinusoidal functions and  $k$  factor), and they consistently attenuate to zero when we approach to circular chief orbit ( $e \rightarrow 0$ ) getting closer to the HCW solution.

In the solution expressions, the  $\delta M$  parameter contains the secular drift because it includes  $\delta a$  as a rate factor multiplying  $M_c(t)$  as an independent variable. The normalized radial position  $\bar{x}$  periodicity is caused by  $\delta e$  and  $\delta M$  multiplying sinusoidals; as the latter parameter contains  $\delta a$ , in a drift condition we have unbounded radial oscillations, as expected from TH-YA. Similar comments (though different

---

<sup>†</sup> Or, alternatively, the difference in true argument of latitude  $\delta \theta$ .    <sup>‡</sup> Or, alternatively, difference in mean argument of latitude  $\delta \lambda$ .

expressions) are valid for the normalized along-track position  $\bar{y}$  periodicity and drift, with the addition of a secular drift summand term<sup>†</sup>.

The radial offset biases are caused by  $\delta a$  and  $\delta e$ , and the along track biases are caused by  $i$  and all **OED** except  $\delta e$  and  $\delta i$ .

The normalized cross-track position  $\bar{z}$  is a decoupled harmonic oscillator reaching a maximum amplitude that increases with  $\delta i$  and  $\delta \Omega$ , at a phase value that depends on the same variables, as expected<sup>‡</sup>.

With the normalized solution equations in **OED** space, it is simple to find maximum deviations in the three relative RTN coordinates, with a given vector of **OED**. This expression is more compact than the dimensional one, but as the chief radius depends on time (general  $e \neq 0$ ), the points of maximum angular separation in the normalized equations doesn't correspond, in general, to the points of maximum physical distance.

As said in answer §3.2.a, the linear mapping between **OED** and relative position and velocity expressed in an RTN frame, holds for any chief orbit eccentricity and yields a better accurate description of the relative motion compared to the **TH-YA** approach, because  $\delta a$  is not approximated by the linearization process.

---

### 3.2.d **OED** description: Chief orbit with small eccentricity

Assuming an intermediate value of eccentricity,  $e > \rho/r \ll 1$  and  $e^2 < \rho/r \ll 1$ , we can simplify the solution, dropping higher order terms on  $e$ . Also, as  $\eta^2 = 1 - e^2 \simeq 1$ , and the chief radius can be approximated as:

$$r = \frac{p}{1 + e \cos f} = \frac{a\eta^2}{1 + e \cos f} \simeq \left( \frac{a}{1 + e \cos f} \right) \cdot \left( \frac{1 - e \cos f}{1 - e \cos f} \right) \simeq a(1 - e \cos f)$$

; then, this enables to de-normalize and obtain simple equations for the dimensional relative position, where we can directly obtain the motion amplitudes in each direction; i.e., the maximum physical separation between **S/Cs**. This is in contrast with the situation for a general eccentricity value, commented in answer §3.2.c.

---

### 3.2.e **OED** description: Chief near-circular orbit

Assuming  $e < \rho/r \ll 1$ , all terms containing the eccentricity can be dropped,  $r \rightarrow a$ ,  $\eta \rightarrow 1$ ,  $f \rightarrow M = nt$ , and sinusoidal phase terms become zero. This yields an expression for the solution of relative motion in this case of near-circular chief orbit, similar to **HCW's** solution.

We can obtain a one-to-one map between **OED** and the **HCW** integration constants. We identify a radial offset in the value  $\delta a$ , corresponding to the radial offset in the original **HCW** solution (previous to apply the "bounded motion" constraint on the initial conditions). There is a term in the along-track direction, proportional to  $\delta M$ , corresponding to the secular drift term in the original **HCW** solution (again, previous to apply the "bounded motion" constraint on the initial conditions). As previously commented, in the **OED** description solution the parameter  $\delta M$  contains a  $\delta a$ -proportional drift term.

We have an offset in the along-track direction that is proportional to  $\delta \omega$  and  $\delta \Omega$ , consistent with the corresponding offset in **HCW**.

The in-plane part of the solution has the periodic motion amplitude proportional to  $\delta e$ .

It has been shown that the numerical simulation of the **OED** description solution is at least an order of magnitude more accurate than the **HCW** solution in cartesian coordinates, and also more accurate than the **HCW** solution in curvilinear coordinates.

---

### 3.2.f **OED** description: Validity of the linearized equations

The typically assumed range of validity of the linearized equations of relative motion is:  $\rho/r \ll 1$

From the simulated examples it seems the order of magnitude of the prediction error over 1 orbit is under 1%.

---

<sup>†</sup> These are "first-look" comments; one should mathematically expand the expressions to clearly identify factors, dependencies, possible terms cancelled, etc. <sup>‡</sup> There is also a dependence on the absolute chief inclination  $i$ , in both amplitude and phase.

### 3.2.g Relative Orbital Elements (ROE): comparison to OED, eccentricity vector and $\delta\lambda$

The ROE state formulation is a nonlinear combination of absolute orbital elements, chosen to be well-behaved in the near-circular chief orbit condition (though it still breaks down in the equatorial orbit case). Since it is desired a nondimensional state vector, the relative semimajor axis has been normalized to the chief's semimajor axis value, to form the element  $\delta a$  of the ROE vector.

Four of its components can be interpreted as two two-dimensional relative vectors, the *eccentricity vector*  $\delta e$  and the *inclination vector*  $\delta i$ , including information of in-plane and out-of-plane relative motion, respectively. This allows for an interesting geometrical interpretation of the relative motion, and is also a powerful tool for FF mission design.

Under non-perturbed Keplerian conditions, all the vector components of the ROE formulation are invariant<sup>†</sup> except  $\delta\lambda$ , the *relative mean longitude* between the S/C vehicles. This relative orbital element variation appears when the energy matching condition is not fulfilled, due to a nonzero difference in semi-major axis that drives a difference in mean motion between the involved vehicles.

### 3.2.h ROE description: mapping with Hill coordinates

The linear mapping between Hill coordinates and ROE has been presented, under the two assumptions of small relative radius compared to chief orbital radius, and near-circular chief orbit. It has the mean argument of latitude  $u$  as the independent variable.

Compared to the HCW mapping it has a similar form, now in terms of the ROE components.

The ROE elements defined by D'Amico have the distinct advantage of matching exactly the integration constants of the HCW approximated formulation. The proposed state and its associated mapping to a relative motion  $[r \ v]^T$  state, can consider the boundness constraint not as approximated conditions but in the essential form of  $\delta a = 0$ . The accuracy is better than in the HCW general solution, as the relative eccentricity vector retains second-order (eccentricity) terms.

Compared to Schaub's mapping approximated for near-circular chief orbit, it has a similar form, now in terms of the ROE components. But now the expressions are inherently linked to the geometry of the relative motion; knowing the three two-dimensional points  $\delta e$ ,  $\delta i$  and  $(\delta\lambda, \delta a)$ , means that we have characterized the shape of the orbit.

### 3.2.i ROE space: Bounded motion and minimum separation

In ROE space, we can achieve bounded and centered relative motion when drafting the orbit geometry, directly in function of the ROEs as drivers of the shape, shift and orientation of the relative orbit. This stands in contrast, for example, with the cartesian  $[r \ v]^T$  chief-centered RTN space, where it is required to verify restrictions on the initial conditions in that cartesian frame.

In the case of bounded relative motion, the analytical expression for the minimum separation perpendicular to the flight direction, is:

$$\delta r_{nr}^{min} = \frac{\sqrt{2}a|\delta e \cdot \delta i|}{\sqrt{\delta e^2 + \delta i^2 + |\delta e + \delta i| \cdot |\delta e - \delta i|}}$$

It can be proven that if we define (at orbit design time) the vectors  $\delta e$  and  $\delta i$  to be parallel (or anti-parallel), then we will have a guaranteed minimum separation between vehicles, on the chief's cross-track plane. This minimum separation value is maximized when the length of the shortest of these two vectors is maximized.

### 3.2.j ROE space: Relative perigee and relative ascending node

We keep considering an RTN frame fixed to the chief vehicle. For simplicity in the description we assume  $\delta a = 0$ , then there is no offset in radial direction and no drift in along-track direction.

The *relative perigee*  $\varphi$  and *relative ascending node*  $\vartheta$  determine particular angular locations in the relative orbit, and also are the phases of the  $\delta e$  and  $\delta i$  vectors, respectively.

When  $u = \varphi$ , it can be seen that the coordinate in the radial direction takes its lower value. The deputy S/C is located right below the center, so this phase angle is called *relative perigee*.

When  $u = \vartheta$ , it can be seen that the coordinate in the cross-track direction reaches zero. The deputy S/C is just crossing the chief's absolute fundamental orbit plane in the direction South→North, so this phase angle is called *relative ascending node*.

<sup>†</sup> In particular,  $\delta e$  and  $\delta i$  vectors can be visualized at static points on  $\mathbb{R}^2$  plane.

For parallel relative eccentricity and inclination vectors,  $\varphi = \vartheta$  ; i.e., it is the line of intersection of both orbital planes at which the cross-track separation is zero.

The deputy vehicle trajectory direction (clockwise or counter-clockwise) in each plane projection depends on the sign of the phase difference  $\varphi - \vartheta$  ; i.e., the quadrants where the vectors  $\delta e$  and  $\delta i$  are located.

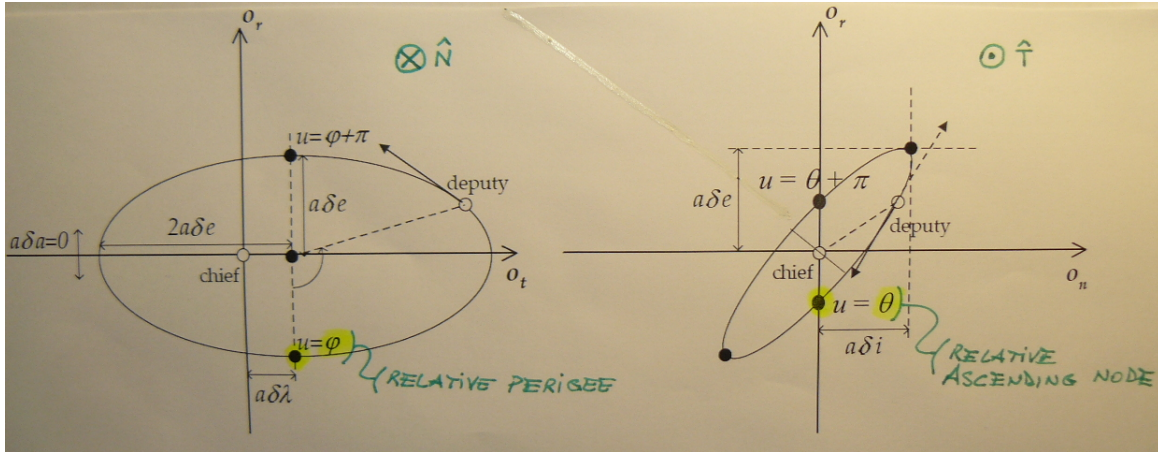


Figure 1: Relative perigee and relative ascending node

### 3.2.k ROE space: Safe/unsafe formations and small baselines

Specifying a worst-case bound  $d_{min}$  for the particular space mission, then the evaluation of the expression for  $\delta r_{nr}^{min}$  shall verify the rigorous limit:

$$\delta r_{nr}^{min} \geq d_{min} \Leftrightarrow \text{SAFE}$$

$$\delta r_{nr}^{min} < d_{min} \Leftrightarrow \text{UNSAFE (forbidden configuration)}$$

For a given mission requirement  $d_{min}$ , we have  $\delta r_{nr}^{min}(\delta e, \delta i, \varphi - \vartheta) = d_{min}$  as the safety threshold. We can visualize this condition in  $\mathbb{R}^3$  space, as a level surface of the function  $\delta r_{nr}^{min}(\delta e, \delta i, \varphi - \vartheta)$ . Considering the variable  $(\varphi - \vartheta)$  in the vertical axis of the plot, the safe configuration condition spans all 3-tuples below the surface and down to  $(\varphi - \vartheta) = 0$ .

We can obtain smaller baselines in the TR plane by a proper selection of the angle enclosed between relative eccentricity and relative inclination vectors. The size of the orbit in the along-track (TR) plane is given essentially by  $\delta e$ . The intersection between the level surface for our safety threshold and a plane defined by a given<sup>†</sup> constant  $\delta i$ , is a 2D curve separating safe and unsafe combinations of 2-tuples  $(\delta e, \varphi - \vartheta)$ . Then, if we choose a smaller  $\delta e$ , we will need to adjust  $(\varphi - \vartheta)$  accordingly, to a lower value (due to the limiting curve shape).

As a numerical example, in class we have seen the specific case of  $a\delta e = 300\text{m}$ , which is unsafe with  $\varphi - \vartheta = 70^\circ$ , and could be reduced to 250 m if the angular separation between  $\delta e/\delta i$  is specified to be  $20^\circ$ .

## Problems set 4 (assumption: near-circular orbit)

### 4.1.a Perturbations: LEO and GEO

In LEO, except for the approximations of constant differential drag and differential solar pressure, the magnitude of the relative accelerations caused by perturbations are monotonic functions of the relative

<sup>†</sup> This could be a mission requirement, for example.

spacecraft separation. The differential drag is typically two orders of magnitude smaller than contributions from  $J_2$ , but with vehicles in a very close formation this difference can get considerably smaller.

For a **S/C** separation of 1 km, the magnitude of the differential accelerations caused by individual perturbations are:

- **Spherical Earth, 1<sup>st</sup> order.**  $\sim 10^{-3}\text{m/s}^2$ . Only first order terms, linearization (**HCW** approx.).
- **Non-Spherical Earth,  $J_2$ .**  $\sim 10^{-6}\text{m/s}^2$ . Earth's oblateness;  $J_2$  zonal coefficient.
- **Spherical Earth, 2<sup>nd</sup> order.**  $\sim 10^{-7}\text{m/s}^2$ . Including second order terms in separation.
- **Drag, **WC**.**  $\sim 10^{-8}\text{m/s}^2$ . Ballistic coefficients  $\delta B/B = 100\%$ , different **S/C** attitudes.
- **Non-Spherical Earth,  $J_3$ .**  $\sim 10^{-9}\text{m/s}^2$ . Earth's oblateness;  $J_3$  zonal coefficient.
- **Drag, realistic for twin **S/C**.**  $\sim 10^{-9}\text{m/s}^2$ . Ballistic coefficients  $\delta B/B = 2\%$ .
- **Solar radiation pressure.**  $\sim 10^{-16}\text{m/s}^2$  (negligible). Different solar pressure acting on each **S/C**.

The most relevant perturbations are, in order of decreasing incidence: spherical earth first order approximation, non-spherical Earth  $J_2$ , spherical earth second order approximation, drag, non-spherical Earth  $J_3$ . Depending on the specific application we could trade-off between the inclusion of the differential specific accelerations due to drag (non-conservative, high modeling errors) and  $J_3$  (conservative, mainly secular periodic effects) perturbations. Usually, due to its nature, more efforts are put in modeling and including differential drag.

In **GEO**, Earth's conservative gravitation effects have a lower effect due to the higher altitude. Then, the non-conservative differential specific accelerations due to solar radiation pressure become stronger, in relative terms. This implies less formation control accuracy. It also becomes important to include the Moon and the Sun's third-body perturbation effects.

#### 4.1.b Earth's oblateness: Zonal $J_2$ perturbations

We include Earth's oblateness  $J_2$  perturbations in the relative dynamics model, by means of applying the averaging theory to the **LPE** equations. This can be solved in closed form, delivering the time evolution of the mean absolute **OE**, as affected by  $J_2$ .

Then we can replace in our **ROE** definition, assume small separation and near-circular chief orbit (so linearize neglecting second-order terms) and obtain the time derivative of the **ROE** vector, where we can identify the secular variations caused by  $J_2$  effects. The known secular effects of  $J_2$  on each absolute orbit mean **OE**s  $\{\Omega, \omega, M\}$ , has been translated in secular effects on the relative orbit elements  $\delta\lambda$ ,  $\delta e$  vector, and  $\delta i_y$  component of the  $\delta i$  vector.

After integration, we obtain how each **ROE** component, as a function of  $u(t)$ , is affected by  $J_2$  effects. Replacing these vector components in the linear mapping between Hill coordinates and **ROE**, results in a relative motion model which constitutes a first order approximation of the solution to the equations of relative motion, in the presence of  $J_2$  perturbations.

Apart from  $\delta a$  and  $\delta i_x$ , all the **ROE** elements show a secular trend directly proportional to  $J_2$  and the elapsed time  $(u(t) - u_0)$ . The relative eccentricity vector evolves<sup>†</sup> rotating with angular velocity  $\varphi'$ , on an origin-centered circle of radius  $\delta e$ . The relative inclination vector variation is associated to a secular shift of the orbital planes, through a linear drift term on  $\delta i_y$ . Graphically, in the  $\delta i$  associated plane, this represents a variation on a vertical line.

#### 4.1.c Relative eccentricity vector rotation

Assuming a typical **LEO** Earth Observation mission (sun-synchronous 700 km orbit,  $i \simeq 100^\circ$ , orbital period  $T \sim 100$  min), in an interval of 15 days the relative eccentricity vector (rotating with a period  $T_e \simeq 1000T \simeq 70$  days) can rotate an amount of  $\sim 77^\circ$ .

The motion is counterclockwise for inclinations lower than the critical angle:  $(\varphi' > 0) \Rightarrow i \lesssim 63^\circ$ .

The  $J_2$  effect is removed ( $\delta e$  ceases to rotate) at the critical inclination angle:  $(\varphi' = 0) \Rightarrow i \simeq 63^\circ$ . This can be understood in terms of each absolute orbit, remembering from the application of the averaging theory within **LPE**, there exist a drift in the argument of perigee (rotation of the line of apsides) that depends on the inclination angle, and is nullified for the same critical value required in this context to stop the rotation of  $\delta e$ .

<sup>†</sup> On its associated mathematical plane.

#### 4.1.d Relative eccentricity vector rotation

This question is repeated; see: §4.1.c.

#### 4.1.e Relative inclination vector translation

Regarding the drift accumulated along 15 days in LEO, it depends on the value  $\delta i_x = \Delta i$  for the operating scenario. I couldn't estimate a value from the equations at this moment because, embarrassingly enough, haven't found even a crude approximation for the Earth's oblateness effect's coefficient  $\gamma$  in a typical LEO scenario. Apologies for this, as I'm new to this field. However, from a formation-keeping control window setup documented in a paper<sup>†</sup>, considering a configuration with  $a\delta i_x = a\Delta i = 150$  m, there is a variation of  $a\Delta\delta i_y \simeq 1.2$  m for a time interval of 200 min between pairs of cross-track maneuvers. Then, from this information, it can be estimated a total drift of  $a\Delta\delta i_y \simeq 130$  m in this configuration, along 15 days of operations without applying corrective maneuvers.

The direction of movement of the vertical drift in the  $\delta i$  vector depends on the sign of its component  $\delta i_x$ , moving upwards when  $\delta i_x > 0$ ; i.e., when the vector lies on the first and four quadrants of the plane.

The  $J_2$  effect on the inclination vector is removed when  $\delta i_x \triangleq \Delta i = i_d - i = 0$ ; i.e., if we design the formation with the same absolute inclination for deputy and chief vehicles.

At formation design time, we could achieve a desired cross-track baseline (motion amplitude proportional to  $\delta i$ ) by selecting a proper  $\Delta\Omega = \Omega_d - \Omega$ , while at the same time defining  $i = i_d$  to nullify the drift on the inclination vector.

#### 4.1.f Relative mean longitude translation

In a typical LEO scenario ( $\sim 14.4$  rev/day), for each effect we would have the following.

- **Kepler effect contribution.** Assuming  $\delta i_x = 0$ , the only contribution to  $\delta\lambda$  drift is due to a relative semimajor axis being different from zero. For  $\delta a = 1 \cdot 10^{-6}$ ,  $a = -7078135$  m, in 15 days we would get the following variation:

$$a\Delta\delta\lambda = -a(3/2)\delta a\Delta u = (-7078135 \text{ m})(3/2)(1 \cdot 10^{-6})(15 \text{ day})(2\pi/\text{rev})(14.4 \text{ rev/day}) \\ \simeq -14400 \text{ m}$$

- **Earth's oblateness ( $J_2$ ) effect contribution.** Assuming  $\delta a = 0$ , the only contribution to  $\delta\lambda$  drift is due to  $\delta i_x \neq 0$ . As mentioned in §4.1.e, having no estimate for  $\gamma$  at hand, in this case I refer to simulation data obtained from one of the earliest reports in this subject<sup>‡</sup>: For  $a\delta i_x = 500$  m,  $a\Delta\delta\lambda \simeq 100$  m in 20 revolutions. Thus, in 15 days we would get the following variation:

$$a\Delta\delta\lambda \simeq \frac{100 \text{ m}}{20 \text{ rev}}(15 \text{ day})(14.4 \text{ rev/day}) \simeq 1100 \text{ m}$$

The  $J_2$  effect is removed when  $\delta i_x \triangleq \Delta i = i_d - i = 0$ ; i.e., if we design the formation with the same inclination angle for deputy and chief absolute orbits.

Looking at the equation for the drift summand components of  $\delta\lambda$ , we identify that we could mathematically compensate a Kepler contribution  $\delta a \neq 0$  with a  $J_2$  effect contribution of opposite sign enabled through a  $\delta i_x \neq 0$  component in the ROE vector<sup>§</sup>. However, we must be aware that doing this the value  $\delta i_x \neq 0$  generates a drift on the relative inclination vector plane. So, the theoretical way to achieve a bounded relative orbit would be to set  $\delta a = 0$  to cancel Kepler's contribution to drift on  $\delta\lambda$ , and also set  $\delta i_x = 0$  to cancel both  $J_2$  contributions to drift on  $\delta\lambda$  and  $\delta i$ .

#### 4.1.g Differential drag effects

The differential drag causes two relevant secular effects on ROE vector components: a linear increasing secular drift on  $\delta a$ , and a quadratic secular drift on  $\delta\lambda$ .

Geometrically, on ROE plane ( $\delta\lambda, \delta a$ ), the behaviour is as follows with reference to Fig. 2. Starting from point (1) with  $\delta a > 0$  (deputy above the chief) and  $\delta\lambda = 0$ , we assume that the Kepler effect

<sup>†</sup> D'Amico S., Ardaens J.-S., *Spaceborne Autonomous Formation-Flying Experiment on the PRISMA Mission*, AIAA-JGCD Vol. 35, No. 3, 2012. <sup>‡</sup> D'Amico, S., *Relative Orbital Elements as Integration Constants of Hill's Equations*, Report TN-05-08, DLR, 2005. <sup>§</sup> This is very interesting, but it would require the precise in-flight estimation of the effective  $\delta a$ , and also consideration of the difference in order of magnitude between  $\delta i_x$  and  $\delta a$ .

is producing a displacement to the left but, at the same time,  $\delta a$  is decreasing (deputy approaching chief,  $a_d \rightarrow a_c$ ) and then the rate of change of  $\delta\lambda$  is decreasing, so the trajectory goes down describing a curve (point (2)). In point (3), both semimajor axes are actually equal and  $\delta\lambda$  is at a stationary point. After that  $\delta a < 0$ , the deputy gets below the chief (point (4)), still  $\delta a$  keeps decreasing as a real number and  $\delta\lambda$  is decreasing at a rate that increases because  $|\delta a|$  is increasing. The deputy, now being faster, is being increasingly affected by the drag, eventually going back to the opposite side. Indeed, it can be seen that this is a periodic behaviour describing a limit cycle.

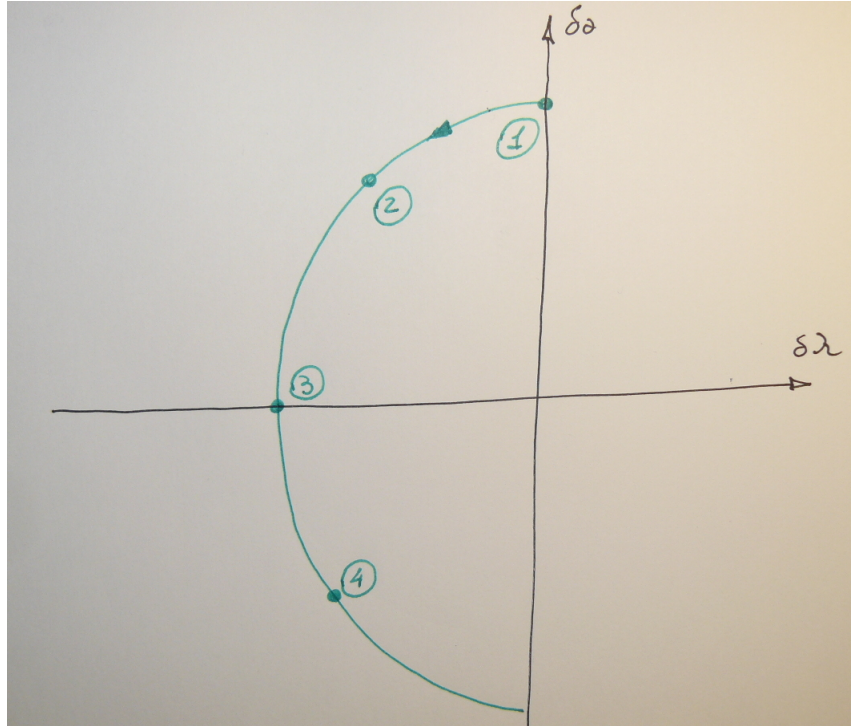


**Figure 2:** Differential drag effects on  $(\delta\lambda, \delta a)$  plane

For closely flying identical S/C in LEO, considering a realistic differential drag coefficient matched to  $\delta B/B \sim 2\%$  (1% matching at launch and 1% total variation during lifetime), in nominal/science mode the differential accelerations are negligible. This situation changes during safe/hold modes (each vehicle with different attitude, in general), arising noticeable differential accelerations.

#### 4.1.h Impulsive maneuvers in the relative dynamics

To incorporate impulsive maneuvers in the relative dynamics model (assuming short relative distances and near-circular chief orbit) we consider an “inverse” equation, obtained in the HCW framework, that relates the integration constants as functions of the relative position, relative velocity (both expressed in a chief-fixed RTN frame), and a generic time. We consider the following:

- The ROE vector components are equivalent to the mentioned integration constants;
- Maneuvers of impulsive nature<sup>†</sup>; i.e., in each RTN direction:  $\delta r = 0$  and  $\delta v$  is a constant value;
- We look for the ROE variation in a given time interval, considering  $u_0 = u(t_0 = 0) = u_M$  the place in orbit of a maneuver occurrence, and the effects of the maneuver after an elapsed time at another location  $u(t) = u$ .
- Use of  $u(t)$  as the independent variable (instead of  $t$ ).

The set of equations derived from these considerations provides a mapping  $\{\delta v\} \leftrightarrow \{\Delta[\delta\alpha]\}$ , enabling us to obtain the actual ROE variation, over an interval elapsed from the maneuver placement to a

<sup>†</sup> Constant  $\delta v$  increments over a very short (“discontinuous”) transition interval, while considering  $\delta r = 0$ . In practice, we consider as “impulsive” such maneuvers of duration much shorter than the orbit’s period.

given epoch. In fact, these equations are equivalent to the integration of the [GVE](#), within our simplifying assumptions.

This is an ideal framework to design closed-form deterministic impulsive maneuvering schemes.

As a brief summary of these equations' implications, the control problem is fully decoupled with respect to in-plane and out-of-plane motions (as expected). A thrust in cross-track direction affects only the  $\delta i$  vector, while a thrust entirely contained in the chief's orbital plane influences:  $\delta e$  vector,  $\delta \lambda$  and  $\delta a$  (the latter is unaffected by  $\delta v_n$ , though). It can be shown that this decoupling is made possible by the specific choice of  $\delta \lambda$  as a relative orbital element.

#### 4.1.i Importance of a closed-form solution of the relative motion control problem

The required delta-v budget for formation keeping can be expressed in terms of [ROE](#), and is directly proportional to the relative eccentricity offset.

At the mission planning stage, we can assess the feasibility of a given stringent requirement on the formation accuracy, according to the [S/C](#) propulsion system limitations.

#### 4.1.j Closed-form minimum delta-v solution for out-of-plane control

Analytically, looking at the corresponding equations (for  $a\Delta[\delta i_x]$  and  $a\Delta[\delta i_y]$ ) affected by a cross-track maneuver, we have two equations and two unknowns that can be solved in closed-form. Then, one cross-track maneuver is necessary and sufficient to control the out-of-plane relative motion. The solution ( $\delta v_n, u_M$ ) is given directly in terms of the required  $\Delta[\delta i]$  correction vector in the relative inclination vector's plane. The delta-v impulse is directly proportional to the norm of the mentioned correction vector (and also to  $n$  and  $a$ ), while the maneuver location is its phase angle.

It would be straightforward to sketch out this graphically, drawing a pre- and post- maneuver  $\delta i$  vector, while its difference is the  $\Delta[\delta i]$  correction vector. For out-of-plane formation keeping, we could draw a "control window" consisting of a circle of allowed variation of the inclination vector, around a nominal value. For example, assuming we are being affected by  $J_2$  effect, whenever the vertical translation  $\delta i$  moves and touches the circular window's boundary, the navigation system informs this to the control system, that applies an impulsive maneuver (with appropriate magnitude and location) to move  $\delta i$  in the opposite direction; i.e., a vertical  $\Delta[\delta i]$  correction vector whose length is the circle's diameter value.

#### 4.1.k Closed-form minimum delta-v solution for in-plane control (two pulses)

Analytically, looking at the corresponding equations (for  $a\Delta[\delta a]$ ,  $a\Delta[\delta \lambda]$ ,  $a\Delta[\delta e_x]$  and  $a\Delta[\delta e_y]$ ) affected by along-track and radial maneuvers, we have four equations and three unknowns, an over-determined system of equations. We can double the number of unknowns seeking for a double-impulse solution and after some math manipulation, simplified by assuming no drift in  $\delta \lambda$  due to a given  $\delta v$ , obtain four expressions: delta-v radial and along-track for both maneuvers. These equations are expressed as functions of their location on orbit and the desired [ROE](#) corrections. A typical solution (out of the infinite possibilities in these four delta-v equations) could be obtained by posing an optimization problem, minimizing a cost functional on  $\delta v$ . The solution has a simple expression, the two maneuvers have only along-track components ( $\delta v_r = 0$ ) with the same magnitude (and opposite sign) of  $(na/4)\Delta[\delta e]$ . I.e., it is proportional to the norm of the required correction vector,  $\Delta[\delta e]$ . The location on orbit of the first maneuver is directly the phase of the latter correction vector, while the second maneuver is located half an orbit later.

In practice, besides being considered constant during the process,  $\delta \lambda$  (tightly coupled to  $\delta a$ ) is unavoidable modified. It can be shown that we can correct for this by adding an appropriate tiny correction summand  $\Delta[\delta a]$  term to  $\Delta[\delta e]$  on the  $\delta v_t$  expressions for both maneuvers.

It would be straightforward to sketch out this graphically, based on the previous description. Analogously to the inclination vector case, we could set-up a control window around a nominally required eccentricity vector. E.g., consider the  $J_2$  effect causing a rotation of the eccentricity vector, and then the control system "kicking it back" with the appropriate correction vector (and appropriate pair of maneuvers ( $\delta v_t, u_M$ )<sub>1,2</sub> according to the previous description), whenever the navigation system reports that  $\delta e$  has reached the boundary of the window.

#### 4.1.l Closed-form minimum delta-v solution for in-plane control (three pulses)

It is mathematically feasible a solution using 3-tuple maneuvers, with corresponding expressions for the required impulses. The solution is optimal on delta-v cost, giving a  $\delta v$  lower bound proportional to the maximum between the norm of the correction in eccentricity vector and the absolute value of the correction in the relative semimajor axis. Currently, there's a closed-form solution only for the case where  $\|\Delta[\delta e]\| > |\Delta[\delta a]|$ . The location of the maneuvers is within a separation of half an orbit, starting from the phase of the required correction in the eccentricity vector.

#### 4.1.m Generalization of the closed-form solution approach, for large reconfigurations

It is hard to find an optimal solution for an arbitrarily large reconfiguration, when including all the perturbations. The problem is divided in two domains: A guidance problem and a control problem.

The guidance problem, spanning a wide timeframe, seek for intermediate configurations of a large guidance plan between an initial and a final ROE state vector, including all perturbations pertinent to the particular application. For this, we consider small “jumps” in the ROE vector, corresponding to each segment of the total state-space path, between “waypoints”. These jump contributions are linearly propagated through a complete STM, to the final time instant. From the GVE equations, we know that the segments correspond to the cost; we need to minimize the path length.

The control problem seeks for maneuver size and location (separately for in-plane and out-of plane decoupled motion) to accomplish each single reconfiguration on a short, limited time span, where we neglect the perturbations and only take into account Kepler's effect. For this, each computed  $\delta v$  is linearly propagated to the state variation through the appropriate control and state transition matrices.

#### 4.2.a Classical formation-flying configurations in LEO

A brief description of some reference trajectories in terms of ROE elements, is the following.

- **Along-Track Orbit (ATO).** A formation with only a separation in along-track direction. I.e.,  $\delta\lambda \neq 0$ ,  $\delta e = \delta i = 0$ ,  $\delta a = 0$  (no drift). Setting  $\delta M \neq 0$ , then we get  $\delta u \neq 0$  and  $\delta\lambda \neq 0$ .
- **In-Track Orbit (ITO).** Chief and deputy S/Cs sharing a common ground-track, through a cross-track separation that compensates for Earth's rotation. For this,  $\delta\Omega = \omega_E \delta\lambda/n$ ,  $\delta u = (1 - \omega_E \sin i/n)\delta\lambda \Rightarrow \delta i_y = \delta\Omega \sin i \neq 0$ ,  $\delta\lambda \neq 0$ . The last two conditions ensure a given baseline with the same ground-track. Note that it is achieved without a difference in inclination, so it is not expensive.
- **General Circular Orbit (GCO).** A 3D circular orbit (projected as an ellipse), centered in the Chief. Setting  $\delta i = \sqrt{3}\delta e$ ,  $\varphi = \vartheta \Rightarrow$  3D circle with radius  $2\delta e$ .
- **Projected Circular Orbit (PCO).** A 2D circular orbit (TN projection), centered in the Chief. Choosing  $\delta i = 2\delta e$ ,  $\varphi = \vartheta + \pi/2 \Rightarrow$  2D circle with radius  $2\delta e$ .

#### 4.2.b Interferometric baseline for DEM through SAR

The baseline for DEM mapping through bistatic SAR interferometry, is defined as the projection of the relative SAR antenna (i.e., S/Cs) positions, perpendicular to the flight and target directions.

We can build such a baseline and modify it regularly in a low cost and low risk manner. By designing the formation and the required configurations during the mission lifetime in terms of ROE vector state-space, we can modify phases and angles of the relative inclination and relative eccentricity for a flexible adjustment of the interferometric baseline, always complying with a safety threshold ( $\sim 200$  m in TanDEM-X mission) for the minimum separation perpendicular to the flight direction. If we even require to pass through an unsafe configuration  $\delta e \perp \delta i$  (e.g., when going from parallel to anti-parallel), we can lower the risk incrementing the along-track separation  $\delta\lambda$  during the reconfiguration operation.

#### 4.2.c ROE change during formation maintenance

As previously explained, the relative eccentricity and the relative inclination vectors are mainly affected by drift due to Earth's oblateness ( $J_2$ ) perturbations, the former rotating and the latter translating vertically. There is also, in general, drift on the mean along-track separation (due to Kepler,  $J_2$  and drag), and drift on the relative semimajor axis (due to drag).

The usual practice for formation keeping is to implement a simple scheme, specifying a circular control window centered around each nominal vector  $\delta e^{nom}$  and  $\delta i^{nom}$ , with radius  $\|\delta e^{max} - \delta e^{nom}\|$  and  $\|\delta i^{max} - \delta i^{nom}\|$ . The idea is to allow each vector to freely move due to drift, upon touching the window boundary where the navigation system signals the event to the control system, and this enqueues the corresponding impulse maneuvers of appropriate value, to be applied at the required orbit phasing location.

As we have seen we have decoupled, independent actions for in-plane and out-of-plane correction, the former (triggered by  $\delta e$  reaching its window threshold) requiring a pair of maneuvers and the latter (triggered by  $\delta i$  reaching its window threshold) requiring a single maneuver. In both cases we have closed-form expressions for computing the required maneuvers from the control windows' thresholds.

Also in general, for the in-plane case, we need to correct for  $\delta a$  and  $\delta \lambda$ ; this could be derived from the  $\delta e$  control window. First of all, in practice we can usually neglect the variation of  $\delta a$  due to differential drag. The  $\delta a$  correction is applied directly, and the  $\delta \lambda$  indirectly, by adding a required contribution to the  $\delta a^{man}$  value (after pair of maneuvers) for the buildup of the required  $\delta \lambda$  (due to  $\delta a^{man}$ , differential drag and  $J_2$ ) over a maneuver cycle, effectively keeping  $\delta \lambda$  moving around a nominal value on its own window. That is, we have closed-form expressions for computing  $\delta \lambda_{target}$  from the control window threshold  $\delta e_{max}$ , also for computing  $\delta \lambda_{total}$  from  $\delta \lambda_{target}$ , current  $\delta \lambda$ ,  $\Delta [\delta \lambda]_{\delta v_{1 \rightarrow 2}}$ ,  $\Delta [\delta \lambda]_{\delta a_{1 \rightarrow 2}}$ ,  $\Delta [\delta \lambda]_{drag_{mc}}$  and  $\Delta [\delta \lambda]_{J_2_{mc}}$ , and finally for computing  $\delta a^{man}$  from  $\delta \lambda_{total}$ .

For the pair of maneuvers case, it can be included in the corrections the consideration for the drift of the parameters between both maneuvers. Also, in all cases, the algorithm can easily include a compensation factor in the correction value, to avoid a vector "getting out" its control window while the system is waiting the appropriate orbit location to apply an impulse.

I refer to Fig. 2.11 of S. D'Amico's PhD. Thesis for the sketch of the variation of in-plane ROE elements, over a maneuver cycle.

#### 4.2.d Control windows and/or maneuver cycle for in-plane and out-of-plane control

Regarding the control windows, it was answered in §4.2.c.

Actually, we can link (closed-form expressions) the size of the maneuver cycle (e.g., in terms of number of revolutions between maneuver sets) with the size of the control window; they are directly proportional.

#### 4.2.e Exercise: Cost to keep a relative eccentricity/inclination vector separation

Assume that the formation is under  $J_2$  effects, only.

From the data provided, we have the phase of the relative inclination vector to be  $\vartheta = 90^\circ$ , there's no effect on  $\delta i$  and then  $\delta v_n = 0$ , i.e. the cross-track maneuver cost is zero because we don't need to correct in this direction.

To estimate the cost for the in-plane correction, we can use the approximate expression we have seen for TanDEM-X (a polar orbit,  $i \sim 100^\circ$ ) mission, with  $N = 1$  and updating it for  $\delta e^{nom} = 300\text{m}$ .

$$a\delta e^{max} \simeq \frac{300}{500} 0.936 \text{ m} \simeq 0.5584 \text{ m}$$

$$\delta v_{t_1} = -\delta v_{t_2} \simeq \frac{na\delta e^{max}}{2} \simeq \frac{300}{500} 0.49 \text{ mm/s} \simeq 0.3 \text{ mm/s}$$

#### 4.2.f Control architecture: Autonomous vs ground-in-the-loop

Autonomous onboard embedded control will be unavoidable if we require a high accuracy formation,  $\sim 1$  m error, requiring a short maneuver cycle for formation maintenance. In a ground-in-the-loop approach, we have unavoidable delays between ground communication epochs. We know that designing accurate, numerically stable, fault-tolerant embedded systems for a S/C service platform is typically a hard and expensive task.

When the required accuracy is such that we can tolerate maneuver cycles in the order of days, a ground-in-the-loop architecture (probably executing automated tasks) will be the reasonable choice.

#### 4.2.g Eccentric chief orbit: Minimum-fuel maneuver

Considering an eccentric chief orbit, the minimum-fuel maneuver to establish bounded relative motion, i.e. correcting  $\delta a$ , should be performed at periapsis, in along-track direction ( $\delta v_r = 0$ ). This is similar to our ROE vector space impulsive control solution (for near-circular orbits) and suggests we can extend it to the eccentric chief orbit case.

The size of the optimal impulse is directly proportional to the required correction on the relative semi-major axis and to the deputy's orbital angular momentum, and inversely proportional to the deputy's orbit eccentricity and to the square of its semimajor axis.

## Problems set 5

### 5.1.a Schaub's algorithm for impulsive control in eccentric orbits

Based in the GVE equations describing the evolution of a classical set of osculating OE subject to specific forces, Schaub proposes the following scheme for impulsive control in eccentric orbits, providing closed-form expressions.

- One cross-track impulse, applied at a certain orbit phase, for correction of the inclination and the right ascension of the ascending node. As we can expect from the GVE, this impulse has a cross-coupling effect on the argument of perigee, then we will need to correct it in a future maneuver cycle.
- Two radial impulses, one applied at perigee and the other at apogee within an orbit period, for correction of the argument of perigee and the mean anomaly. The equation for correction of the argument of perigee must include a summand term ( $-\Delta\Omega \cos i$ ), for compensation of the cross-coupled effect when correcting for  $\Delta\Omega$  and  $\Delta i$ .
- Two along-track impulses, one applied at perigee and the other at apogee within an orbit period, for correction of the semimajor axis and the eccentricity.

The mean OE errors are established at some arbitrary point in the orbit, and are then held constant during the orbit while appropriate  $\Delta v$  are applied. Short-period effects are neglected. This impulsive firing scheme assumes that all of the mean OE errors will remain constant over an orbit. In general,  $\Omega$ ,  $\omega$  and  $M$  will experience some  $J_2$ -induced secular relative drift, but its effect over one orbit is neglected. Any neglected error evolution over the current orbit can be corrected in the next maneuver cycle.

However, if we have a large  $\Delta a$ , then due to Kepler effect we cannot assume that  $\Delta M$  will be constant over an orbit. The procedure in this case will be to correct in a first orbit for semimajor axis, eccentricity and inclination, and then correct in a second orbit for  $\omega$  and  $M$ . If we correct for  $\omega$  and  $M$  during the first orbit while we have a large  $\Delta a$ , the fuel cost will be higher due to the inappropriate corrections performed on  $\omega$  and  $M$ .

It is claimed that, if several OE are to be corrected, then this method would still yield a near-optimal solution with a fuel cost increase of only a few percent over the multi-impulse optimal solution.

### 5.1.b Schaub's algorithm for continuous control in eccentric orbits

The control tracking errors are computed using mean OE.

The GVE equations refer to osculating OE. The mean OE are a nonlinear function of the osculating OE. We can develop a state-space model for the mean OE state and the same control inputs. We build the dynamics matrix ( $A(e)$ ) with the coefficients obtained from LPE applied with Averaging Theory; i.e., including  $J_2$  secular drift terms. For the control input matrix ( $B(e)$ ), we start from the GVE, use a first-order truncation from Brouwer theory for the osculating/mean mapping, and approximate its Jacobian as

an identity matrix. The latter approximation is equivalent to assume that the osculating OE changes are directly reflected in corresponding mean OE changes.

Finally, the dynamics of the control error is computed from this model, using mean OE.

### 5.1.c Schaub's algorithm for continuous control in eccentric orbits (Lyapunov)

- (a) The feedback control law will provide asymptotic stability, if and only if:

$$B\mathbf{u} = -(A(\hat{\mathbf{e}}_d) - A(\mathbf{e}_d)) - P\Delta\mathbf{e}$$

, where the feedback gain matrix is required to be  $P > 0$ .

Since the system of equations is over-determined, when we solve for the control input it is required to use a pseudo-inverse matrix. Because of this, the obtained control is no longer guaranteed to satisfy the stability constraint, but numerical simulations indicate its stability, effectively cancelling mean element tracking errors.

- (b) The Lyapunov control design method does not give performance measures on the obtained control law. For this, we have the degree of freedom given by the required  $P(t) > 0$ . Looking at the GVE equations, we can build  $P$  heuristically for performance; e.g., a diagonal matrix with gain elements that are maximum when the corresponding OE are the most controllable. Alternatively, we could pose an optimization problem on this matrix, to minimize some desired cost function.

- (c) For mean OE control, the control tracking error is computed in the following way. On one side, the navigation system provides cartesian position and velocity for the deputy S/C, then we convert it to (absolute) osculating OE, and then to (absolute) mean OE. The later conversion is done with a first-order (Brouwer theory, including  $J_2$  effects) truncated mapping. As a result, we obtain the "true" (deputy) mean OE. On other side, the same steps are done to obtain the (absolute) mean OE for the chief S/C, from its cartesian position and velocity vector provided by the navigation system. If we sum to the chief's (absolute) mean OE a *desired* mean "difference" OE, then we obtain the desired (absolute) mean OE for the deputy. Finally, we subtract the latter "desired" (deputy) mean OE variable from the previously obtained "true" (deputy) mean OE, obtaining the control tracking error in terms of mean OE. Assuming proximity between S/Cs, the errors introduced by the osculating to mean OE approximated transformation are similar (to first order) for both vehicles, so they are cancelled in the final subtraction to obtain the tracking error.

If we want to design a Lyapunov controller in cartesian space, then we will need to build an appropriate cartesian control tracking error. This is done with the construction shown in the block diagram of slide number 14 of lecture 9. This is more complex because, for both vehicles, we need to go forward and backward from cartesian space to mean OE space. On the branch of the diagram that starts from the chief S/C cartesian vectors, we need to build the desired deputy vector in the mean OE space, including  $J_2$  effects in the transformation, and get back to cartesian space. On the branch of the diagram that starts from the chief S/C cartesian vectors, we need to perform the same transformation steps in order to look for a later cancellation of the mappings' approximations, when computing the final tracking error.

- (d) From the numerical simulations case results, we see that the performance is similar between cartesian feedback and mean OE feedback, though the former approach takes a little longer to converge, oscillating during the process. However, after reaching steady-state, the detailed behaviour of the tracking error looks better for the cartesian feedback case.

In general, the cartesian state has a fast moving instantaneous point information, while the OE state has a slower orbital memory information. This difference in information time scale gives the dissimilar convergence times. It should be mentioned that numerical difficulties may arise with the scheme based in cartesian control, due to the approximations introduced by the implementations of the osculating-to-mean and mean-to-osculating OE mappings.

### 5.1.d Virtual telescope in Earth orbit

Topic not covered.

### 5.1.e Virtual telescope in Earth orbit (II)

Topic not covered.

### 5.2.a Metrology systems used for spacecraft formation-flying and rendezvous

Some key metrology systems, are: gyroscope and accelerometer clusters for attitude determination and inertial determination of position and velocity, star tracker for attitude determination, GNSS receivers for position/velocity/time/attitude determination, telegoniometers for range and line-of-sight determination.

### 5.2.b Need for relative navigation

A real-time relative navigation system is needed onboard a S/C vehicle, in order to estimate the current state representation for our relative orbit, and feed it to the guidance and control system.

Besides numerical simulation purposes, an on-ground relative navigation system, appropriately feeded with real sensors data<sup>†</sup>, is a useful tool for obtaining more accurate post-facto estimations of the chosen state representation.

### 5.2.c Basic processing methods for absolute/relative orbit determination

The two basic groups of processing methods for absolute or relative orbit determination, are: batch estimation and sequential estimation of the state vector.

In batch (least squares) estimation, all the available observations are processed and combined to obtain each single state vector. It is suited for on-ground post-processing (smoothing) of all the available data, in order to achieve estimates of high accuracy, being also robust to detect outliers, though it takes a long time to converge.

The sequential estimator obtains a new estimate of the state vector after each observation, uses only information from the past, converges quickly (at the expense of stability) and is required for causal real-time onboard implementation on an embedded fault-tolerant computer with limited computing power.

The deterministic methods, relying on a reference rough orbit estimate, could provide a solution but can't cope with uncertainties (for both the dynamic model and the measurements) and doesn't provide a mechanism to augment the state vector.

### 5.2.d Filter used for onboard navigation

The most adopted filter used for onboard navigation is the Kalman Filter (KF). Since the basic form of this estimator is stated in the context of linear state-space but our problem can be modeled by nonlinear state and measurements equations, usually a linearizing version of the filter is applied; here we will consider the use of the Extended Kalman Filter (EKF).

For the application of the discrete-time KF as a state estimator, we start modeling the state evolution and its measurements as an LTV-stochastic system with deterministic input  $\{\mathbf{u}_k\}$ :

$$\Sigma (k \geq 0) : \begin{cases} \mathbf{x}_{k+1} = F_k \mathbf{x}_k + W_k \boldsymbol{\xi}_k + B_k \mathbf{u}_k \\ \mathbf{y}_k = H_k \mathbf{x}_k + \boldsymbol{\eta}_k + D_k \mathbf{u}_k \end{cases}$$

, usually tied to the following assumptions on the involved stochastic processes:

**h0)**  $\{\boldsymbol{\xi}_k\} \in L^2(\mathbb{C}^p)$  ,  $\{\boldsymbol{\eta}_k\} \in L^2(\mathbb{C}^q)$  ,  $\{\mathbf{x}_k\} \in L^2(\mathbb{C}^n)$ .

**h1)**  $\mathbf{E}[\boldsymbol{\xi}_k] = \mathbf{0}_p$  ,  $\mathbf{E}[\boldsymbol{\eta}_k] = \mathbf{0}_q$  ,  $\forall k$ .

**h2)**  $\mathbf{E}[\boldsymbol{\eta}_k \mathbf{x}_0^*] = \mathbf{0}_{q \times n}$  ,  $\mathbf{E}[\boldsymbol{\xi}_k \mathbf{x}_0^*] = \mathbf{0}_{p \times n}$  ,  $\forall k$ .

**h3)**  $\mathbf{E}[\boldsymbol{\xi}_l \boldsymbol{\eta}_k^*] = \mathbf{0}_{p \times q}$  ,  $\forall k, l$ .

<sup>†</sup> I.e., data acquired from telemetry of the real S/Cs.

$$\mathbf{h4)} \quad \mathbf{E} [\boldsymbol{\eta}_k \boldsymbol{\eta}_l^*] = R_k \delta_{kl} = \begin{cases} R_k > 0, k = l; \\ \mathbf{0}_{q \times q}, \forall k \neq l. \end{cases}$$

$$\mathbf{h5)} \quad \mathbf{E} [\boldsymbol{\xi}_k \boldsymbol{\xi}_l^*] = Q_k \delta_{kl} = \begin{cases} Q_k > 0, k = l; \\ \mathbf{0}_{p \times p}, \forall k \neq l. \end{cases}$$

If we add the assumption on the involved noise random sequences having Gaussian distributions, then the **KF** is the optimal (**MSE**) filter. Without this additional assumption, it is the optimal (**MSE**) filter among a class of linear estimators.

Some of the limitations imposed by this set of assumptions can be tackled by re-organizing variables within the same scheme, and augmenting the state vector with new variables to be estimated.

Now consider a nonlinear system model with additive noises, assuming:

**h6)** Nonlinear vector field for the evolution of the state:  $\mathbf{f}_k(\mathbf{x}_k) \in \mathcal{C}^1$ .

**h7)** Nonlinear vector field for the measurements:  $\mathbf{g}_k(\mathbf{x}_k) \in \mathcal{C}^1$ .

With these hypothesis, the classic **EKF** applies a first-order Taylor approximation around the estimate  $\hat{\mathbf{x}}_{k+1|k}$ , to obtain the corresponding matrices for an **LTV** system that is tractable with the discrete-time **KF**. Considering this for each stage of the real-time implementation, then we have:

- In the time update stage, we propagate the state vector and the estimation error covariance matrix by means of the model dynamics: **STM**, process noise and control inputs (and their associated matrices).
- In the measurement update stage, we compute the Kalman gain matrix, we update the state estimate (and the innovations), and we update the (estimation error's) covariance matrix estimate.

The key ingredients necessary to implement the filter, are: the dynamical model, the measurements model, the uncertainty on the state estimate (covariance matrix for the estimation error), the uncertainty on the measurements (covariance matrix for the measurements), the uncertainty on the dynamics (covariance matrix for the process noise).

### 5.2.e Change in the implementation of the filter when changing measurement types

If we change the type of measurements to include raw observables instead of variables more directly related with our state vector, we must update the measurement model (and the associated Jacobian matrix required in the linearization step) accordingly.

In slide 10 of lecture 10 we have seen examples for **GNSS** and optical navigation. In the first example, for a given **GNSS** space vehicle's signal, the partials of the geometric range  $\rho(t)$  w.r.t. the inertial **S/C** position  $\mathbf{r}$  (state) are computed, being approximated by a line-of-sight vector from local **S/C** to the **GNSS** vehicle at sight (expressed in **ECEF** coordinates), mapped to the **ECI** frame with the appropriate **DCM**. The second example shows expressions for the azimuth and elevation partials w.r.t. the relative position in the camera frame, and also expressions for the partials of the line-of-sight vector with respect to the azimuth and elevation angles. These expressions are to be used as factors of a chain's rule and coordinate transformation expression required for building the final measurements sensitivity matrix.

### 5.2.f Goal of TanDEM-X Autonomous Formation Flying experiment (TAFF)

**TAFF** is an embedded autonomous relative control system. Its main objective is to provide, onboard TanDEM-X, a robust control algorithm for formation keeping, and to demonstrate a substitution of ground-based formation control.

**TAFF** performs only the in-plane control of the **S/C** formation.

### 5.2.g TAFF: Characteristics

**TAFF** uses a **ROE** state vector representation.

The observer uses PVT navigation measurements from two Astrium MosaicGNSS (L1, 8 channels, 1 Hz) **GPS** receivers, one locally in TanDEM-X and the other at the remote **S/C**, with data coming through an S-band intersatellite link. A synchronized set of navigation solutions (**ECEF** coordinates) is provided every 10 s to **TAFF**.

The system includes Earth's oblateness ( $J_2$  zonal coefficient) perturbation effects. The differential maneuver execution errors are, in fact, another source of perturbations.

---

### 5.2.h Efficient way to compute relative position and velocity

Instead of building rotation matrices (and their associated computationally expensive multiplications) for all the required transformations, an efficient way to pre-process the position (expressed in **ECEF**) and velocity (measured and expressed in **ECEF**) delivered by the twin **GPS** receivers onboard each **S/C**, is the following.

1. We perform the differences according to our convention, obtaining the relative quantities, and then use the Coriolis theorem in the following way:

$$\Delta \mathbf{v}^{eci} = \Delta \mathbf{v}^{ecf} + \boldsymbol{\omega}_{ecf} \times \Delta \mathbf{r}$$

$$\Delta \mathbf{v}^{eci} = \Delta \mathbf{v}^{rtn} + \boldsymbol{\omega}_{rtn} \times \Delta \mathbf{r}$$

, where the supra-indices in the relative velocities indicate from which frame they are measured. Solving for  $\Delta \mathbf{v}^{rtn}$ , we have:

$$\Delta \mathbf{v}^{rtn} = \Delta \mathbf{v}^{ecf} + \boldsymbol{\omega}_{ecf} \times \Delta \mathbf{r} - \boldsymbol{\omega}_{rtn} \times \Delta \mathbf{r}$$

$$\Delta \mathbf{v}^{rtn} = \Delta \mathbf{v}^{ecf} + (0 \ 0 \ \Omega_{Earth}) \times \Delta \mathbf{r} - n \hat{\mathbf{e}}_N \times \Delta \mathbf{r}$$

2. We build a **DCM** rotation matrix (only one), in order to express relative position and velocity (up to now expressed in **ECEF** coordinates) as coordinates of the RTN frame. This can be done by putting as its columns each of the RTN versors' coordinates in **ECEF** frame. At last, we multiply this matrix to the previously obtained **ECEF** coordinates of relative position and (RTN-measured) relative velocity, to finally have these quantities expressed as coordinates of the chief-centered RTN frame.
- 

### 5.2.i TAFF: Computing the mean argument of latitude

There is a computationally efficient way to obtain the mean argument of latitude, from the position solution (expressed in **ECEF** frame) delivered by the **GPS** receiver of the chief **S/C**. We note that  $u(t)$  is the phase angle of the position vector on the orbit plane, measured from the line of nodes. From the versors perpendicular to the equatorial and orbit planes, we can build another versor perpendicular to them, lying on the line of nodes, by means of the cross product:

$$\hat{\mathbf{j}} = \frac{\hat{\mathbf{e}}_Z \times \hat{\mathbf{e}}_N}{\|\hat{\mathbf{e}}_Z \times \hat{\mathbf{e}}_N\|}$$

With the same methodology we can also build another versor, perpendicular to the one just obtained and to the versor perpendicular to the orbital plane; this versor will be on the orbital plane:

$$\hat{\mathbf{k}} = \hat{\mathbf{e}}_N \times \hat{\mathbf{j}}$$

Then, we see that the mean argument of latitude is just the phase angle between the orthogonal projection of the position vector along the  $\hat{\mathbf{k}}$  direction, and the orthogonal projection of the same vector along the  $\hat{\mathbf{j}}$  direction:

$$u = \text{atan2} \left( \frac{\hat{\mathbf{k}} \cdot \mathbf{r}_{ecf}}{\hat{\mathbf{j}} \cdot \mathbf{r}_{ecf}} \right)$$


---

### 5.2.j TAFF: Maneuvers

The execution of impulsive maneuvers (output of **TAFF's** control system) is incorporated as control inputs through the **GVE** (simplified for a near-circular orbit), in the **EKF** state propagation, at the time update phase.

Regarding the sign of the delta-v vector, with the convention of relative differences of deputy with respect to chief, when the **S/C** performing the maneuver is the chief the sign must be positive. The sign must be negative when the deputy is executing the maneuver.

---

### 5.2.k TAFF: Measurement partials

In TAFF only position synchronous measurements are used.

Regarding the linearization of the measurements function to form the measurements sensitivity matrix, it is worth to note that the position and ROE vectors are taken at the same time, there's no propagation ( $u = u_0$ ).

---

### 5.2.l TAFF: Performance assessment

During the development cycle of the system and after a pure simulations stage, it was built a Hardware In-the-Loop (HIL) FF testbed, as shown in slide 17 of lecture 10. It comprises a powerful desktop computer that simulates the environment, the dynamics, as well as the sensors and actuators with a high degree of precision. It also comprises a resource limited target computer, representative of the onboard computer, on which the flight software is running.

For comparison and error assessment purposes, it is always available in the host computer an accurate "truth model".

The expected navigation and control accuracies are at the meter level (considering a low control period  $N$ ).

Regarding execution time, the complete algorithm is executed within 14 ms, which corresponds to a CPU load of 0.14%, because it is called every 10 s.

## Problems set 6

### 6.1.a Kalman filters: KF, EKF, UKF

The KF is the optimal solution, in a 2-norm sense, for an LTV state estimation problem.

The EKF consists of using the classical KF equations to the first-order approximation of the nonlinear model about the last estimate. The EKF equations are only approximations. The corresponding propagation equations are available only if the estimate belongs to a neighborhood of the actual state.

The UKF, a more recent development, uses a finite number of sigma points to propagate the probability of the state distribution as accurately as possible; in general this performs better than the first-order approximation of the EKF.

The computational complexity of the UKF is claimed to be similar to the EKF complexity, and both are heavier than the basic KF.

---

### 6.1.b Observables used in single-frequency relative GNSS navigation

Starting from the two elementary observables available from a single-frequency GNSS receiver, pseudorange and carrier phase, we can construct the following linear combinations.

We combine observables to take advantage of cancellations of undesired effects present in the raw observables, effectively improving the attainable accuracy.

The GRoup And PHase Ionospheric Correction (GRAPHIC) measurement is built by taking the arithmetic average value of pseudorange and carrier phase of the same receiver, corresponding at the same time instant, for the signal coming from the same GNSS Space Vehicle (SV). It is independent of the ionospheric path delay and halves the thermal noise level of the pseudorange observable.

The Single-Difference Carrier Phase (SDCP) measurement is obtained by doing the arithmetic subtraction of the carrier phase observables of two different receivers, corresponding at the same time instant, for the signal coming from the same SV. Here the satellite clock offset is eliminated, the systematic error is lower (due to common hardware compensation effects), and for small inter-satellite separations the ionospheric path delay could become smaller than the thermal noise.

The Single-Difference Pseudo-Range (SDPR) measurement is formed by doing the arithmetic subtraction of the pseudorange observables of two different receivers, corresponding at the same time instant, for the signal coming from the same SV. It is unbiased but less accurate than the SDCP.

The Double-Difference Carrier Phase (DDCP) measurement is constructed by doing the arithmetic subtraction of two SDCP measurements taken by the same two receivers, at the same time instant, for the signals originated at two different SVs. In this case, the GNSS clock offset and common systematic

errors are completely removed. In particular, hardware dependent line biases present in the **SDCP** ambiguities, which are still float values, are canceled-out in the **DDCP** ambiguities, which are now of integer nature.

The full strength of carrier phase based navigation is revealed in differential applications, which benefit from a high level of common error cancellation and enable a resolution of the unknown carrier phase ambiguity. This enables millimeter to centimeter positioning accuracies.

Finally, it must be noted that when we combine carrier phase uncorrelated random noises in the “difference” data types, then the resulting **SNR** will be 3 dB lower.

### 6.1.c Choosing state parameters and measurement data types

Starting from well understood requirements of absolute and relative navigation and through the real-time navigation system **EKF** design process, we need to choose the appropriate measurements and the state vector components (variables and parameters to be estimated by the filter), and the structure of the **EKF** itself. It is worth to mention that, besides functional navigation requirements, for such a subsystem of a **S/C** we have always a subset of requirements involving reliability, **FDIR** and environmental limitations. Thus, the architecture design of the estimation filter is a trade-off work considering benefits and disadvantages of each choice, with the ultimate goal of fulfilling the requirements while avoiding any unnecessary complexity.

As we have seen, the most accurate **GPS** measurements available which bring along absolute orbit information are the **GRAPHIC** data types, while the most accurate relative navigation observables are the **DDCP** data types. Both data combinations involve the usage of carrier phase measurements and thus require the laborious handling of carrier phase biases, being it float or integer valued. On the other hand, the easiest and least computational intensive approach is to use pseudorange measurements only for absolute navigation, and implicitly derive the relative navigation information by subtracting two absolute filter states. In between these two extremes, ultimate accuracy using  $\rho_{GR}$  and  $\rho_{DDCP}$  or ultimate simplicity using  $\rho_{PR}$ , the optimal design solution is somewhat in the middle.

Clearly, when selecting a given set of observables, this also affects the type and number of parameters to add into the **EKF** augmented state.

Regarding the **EKF** basic architecture, it can be considered a “split” scheme with separated filters for absolute and relative navigation, or a “combined” single filter for estimating both navigation states.

For the **PRISMA** mission, all this data types and architecture alternatives had been evaluated through the building of a comparative table and a decision matrix. It was decided to use a combined **EKF** architecture, with **GRAPHIC** and **SDCP** measurements. As the decision arises from such a large comparison matrix, it would be lengthy to describe here the complete reasoning supporting this choice. Trying to summarize, on one side a robustness and simplicity criteria favored the use of the combined architecture for the filter, as it provides robustness in the case that both **S/C** don't have common **GPS** satellites in view, and it also simplifies the initialization and maneuver handling procedures. On other side, the selected types of measurements (in the context of the selected filter architecture) can meet the application requirements with a reasonable computational load and overall filter complexity that enables it to be carried on the **LEON3/GRLIB FPGA-based SoC**.

The selected filter state vector has the following 49 components:

$$\mathbf{y} = [ \mathbf{r}^m \ \mathbf{v}^m \ \mathbf{p}^m \ c\delta t^m \ N^m \ \mathbf{r}^t \ \mathbf{v}^t \ \mathbf{p}^t \ c\delta t^t \ N^t \ \delta v ]^T$$

This is, for each **S/C** (superscripts  $m$  and  $t$ ): the 6-dimensional cartesian state coordinates expressed in the **ECI** frame, the scalar **GPS** receiver clock offset, a fixed number of force model parameters

$\mathbf{p} = [ C_D \ \mathbf{a}_{emp} ]$  (i.e., aerodynamic drag coefficient and three empirical accelerations in the local orbital frame), and the 12 **GRAPHIC** floating-point biases. Finally, the state is also augmented with the three **Main S/C** orbit maneuver increments, expressed in the local orbital frame.

### 6.1.d PRISMA navigation system

- (a) The **STM** for the selected filter architecture includes the following submatrices:  $\Phi_{23 \times 23}^m$  and  $\Phi_{23 \times 23}^t$  the transition matrices for the uncontrolled orbit motion of each **S/C**, and  $\Phi_{23 \times 3}^{\delta v}$  the transition matrix mapping an orbit maneuver increment at time  $t_M \in [t_0, t]$  to the **Main S/C** orbit motion (position and velocity) at time  $t$ . The  $\Phi_{23 \times 3}^{\delta v}$  is a direct approximation of the partials, its submatrices being proportional to the **DCM** between **RTN** and **ECI** frames, and the  $(t - t_M)$  time interval. The  $\Phi_{23 \times 23}^m$  and  $\Phi_{23 \times 23}^t$  matrices have the same structure, its submatrices  $\Phi^x$  and  $\Phi^{x \cdot p}$  are obtained through the numerical integration of the variational equations (using a full dynamic model, no approximations).

The partials of the force model parameters at time  $t$  with respect to the force model values at time  $t_0$  are given by a (sub)matrix that considers the atmospheric drag as constant in this time interval, and includes a submatrix  $\Phi^{a_{emp}}$  that propagates the empirical accelerations. The GRAPHIC floating-point biases are considered constant over a continuous tracking arc, then they are propagated through an identity matrix  $I_{12 \times 12}$ .

The entries of the  $\Phi_{23 \times 23}^m$  and  $\Phi_{23 \times 23}^t$  STMs relative to the GPS receiver clock offset and to the empirical accelerations  $a_{emp}$  are treated as stochastic variables via the application of dedicated process noise models. Empirical accelerations  $a_{emp}$  (in the three RTN directions), modeled by first-order exponentially correlated (“colored”) noise (with an appropriate correlation time constant of  $\sim 900$  s), are considered to compensate for any modeling deficiencies in the employed S/C dynamics. The receiver clock offset for each S/C is modeled as a random walk stochastic process. These kind of noises, required to be included in our complete model, are not white. Then, in order to comply with the KF assumptions, they are accommodated in the scheme by putting its white part as process noise, and the remaining of the noise model as augmented state parameters and a corresponding part of the STM describing the dynamics of the noise.

The variational equations are a special set of differential equations that enable us to incorporate perturbations using a full dynamic model and, after its numerical integration, obtain a highly accurate STM. It can also be used for the treatment of partials with respect to force model parameters.

- (b) In the measurement sensitivity matrix, the only submatrices which are not constant are those containing the partials of the geometric range vector  $\rho$  with respect of the corresponding S/C position.

The resulting approximated expression of the GPS measurement partials implies the availability onboard of the GPS SVs positions and clock offsets, necessary to compute the position of the SV when the navigation signal was generated, and the spacecraft attitude necessary to take into account the GPS antenna offset (constant lever arm) with respect to the spacecraft center of mass and consequently compute the position of the receiving antenna. The GPS satellite and clock offsets are obtained from the GPS receiver broadcasted ephemerides. The satellite attitude is provided by the AOCS system. Of course, for retrieving the required values from the companion S/C, an intersatellite link is required.

- (c) The mechanization and implementation of the EKF are important aspects to mitigate the possibility of numerical problems.

The “loss of symmetry” phenomenon refers to the estimation error covariance matrix becoming not symmetrical as a result of the nominal EKF computations. In the original formulation of the covariance update equation, numerical errors which affect the arithmetic difference might produce covariance matrices that fail to retain non-negativity and symmetry. This can happen when the filter is close to steady state and tries to update a covariance matrix whose elements are very small.

One way to guarantee the symmetry of the covariance matrix is to use the Joseph’s form in the update stage of the filter’s mechanization, though this imposes more computational load. Other approaches can be performed, mathematically guaranteeing a well-behaved covariance matrix. In D’Amico’s PhD. Thesis, it is proposed a mathematical form that does the job with a lower computational effort than using the Joseph formula, and then is better suited to the real-time EKF implementation.

- (d) The goal is to select an appropriate force model that fulfills the orbit prediction requirements and could be implemented onboard. In particular, the propagated absolute S/C position shall be better than 10/100/5 m (R/T/N, RMS) and the propagated relative position shall be better than 0.5/10/0.5 m (R/T/N, RMS) within a 50 min prediction interval.

Although the force model used to compute the accelerations acting on the S/C has little impact on the achievable navigation accuracy, the choice of the dynamic model is the key driver of the orbit prediction accuracy, because in the absence of valid GPS observables, the measurement update of the EKF can’t be performed and only a time update takes place.

- (e) The main forces acting on a LEO S/C depend on the Earth’s static gravity field, the aerodynamic drag, the third-body perturbations of the Sun and Moon, the solar radiation pressure, the effects of tidal displacements due to solid Earth, polar and ocean tides, as well as on general relativity effects. A “true” reference trajectory is generated through the selection of the best available force model, initial conditions and S/C parameters. The absolute and relative prediction errors are computed by subtracting the position propagated through a “tailored” force model from the true trajectory over 60 min at 10 s intervals. The tailored force model neglects individual force contributions, one

at a time, to evaluate the single effects on the prediction error budget. The prediction error is also influenced by the initial orbit state error, and by numerical integration and interpolation errors. These effects are taken into account indirectly by introducing a conservative margin on the selection of the individual contributions of the filter force model which shall accumulate a prediction error not larger than the requirement divided by ten. Being the relative position errors at the millimeter level, the absolute orbit propagation errors are the drivers of the force model selection.

The truncation of the geopotential harmonics has the major effect on the prediction accuracy; we note it is required to use, at least, a gravity field of order/degree 20 that provides an accumulated error under  $1/5/0.5$  m (R/T/N). Solar and Moon third-body forces and aerodynamic drag accumulates an error budget of  $1.5/3.5/0.5$  m (R/T/N). At last, solar radiation pressure, tides and relativity can be neglected with accumulated errors below 0.5 m and 1 m in radial/cross-track and along-track directions, respectively.

- (f) The navigation system performs a numerical integration of the variational equations jointly with the orbit state vector, using a fourth-order Runge-Kutta method augmented with Richardson extrapolation (RK4R). The adopted integration macro step size is  $H = 2h = 92$  s. A numerical orbit propagation is invoked by the GPS-based Orbit Determination (GOD) after the EKF processing, each 30 s, which results in a set of orbit coefficients. These coefficients allow for a quintic Hermite interpolation of the S/C position and velocity within the interval  $[t_0, t_2 = t_0 + 2h]$ , which is performed by the GOD function to support the EKF time update at the next call (30 s later) and by the GPS-based Orbit Prediction (GOP) function to output both S/Cs orbit states in the ECI and ECEF frames at a 1 Hz rate.

Maneuver incorporation is required in the EKF. When one or both of the spacecraft maneuvers during the prediction time span, several possible methods can be considered to generalize the KF equations. One solution is to adapt the STM assuming a perfect maneuver model with no uncertainties. This approach fails to produce the final covariance matrix in the presence of uncertainties (e.g., maneuver execution errors). Other solution omits the maneuver from the trajectory prediction and schedule the process noise covariance matrix in such a way that it grows in correspondence of the maneuver execution. This method may be desirable when full information regarding the thrusting is unavailable. It can be shown that this approach yields good accuracy for the covariance computation, but fails to model the orbit state in the time update of the EKF. Another approach models the maneuver in the process and takes into account its uncertainty by adapting both the STM and the process noise covariance matrix. The EKF state is augmented to include the maneuver parameters in the estimation process. As a consequence both state transition and covariance matrix are adapted using the a-priori maneuver information. This method provides a combination of good accuracy in the computation of the covariance matrix, the orbit state, and offers at the same time maneuver estimates which may be used for thrust calibration and process monitoring.

- (g) A simulation environment must be developed, for numerical validation of the GPS-based absolute and relative navigation filter functionality and performance, with the aim to verify the assumptions made during the design process, and ensure that the filter design has the potential to meet the requirements. It includes a rigorous force model (with the forces previously selected), an efficient variable order variable step-size multi-step numerical integration method of Shampine/Gordon, and realistic sensor (raw GPS measurements, accelerometers measurements) and actuator (propulsion system) models.

Four test cases have been defined to validate the navigation concept and perform a preliminary assessment of the expected navigation accuracy, aiming to increase the scenario complexity in a stepwise approach and cover the operational configurations that are most likely to be met during flight. First, an open loop scenario is specified, where no orbit control maneuvers are performed and the S/Cs attitude profile is nominal. Second, a closed-loop scenario is presented, where the relative motion is controlled routinely using the algorithms previously developed. Next, operational contingencies are defined, where data gaps have to be autonomously bridged by the navigation software. In particular, long GPS measurements outages are introduced in both the open-loop and closed-loop simulations to assess the robustness and reliability of the GPS navigation concept.

Regarding the EKF tuning, we need to balance it, giving the proper weight (“trusting”) to the dynamical model (“dynamics” behaviour) and the measurements (“kinematics” behaviour). On one side, we know that a “large” initial estimation error covariance matrix  $P_0$  is suitable for the kick-off of the filter. On other side, an appropriate adjustment of the initial measurement covariance matrix  $R_0$  is very important. Both the empirical accelerations exponentially correlated noise and the user clock offset random walk noise need to have an appropriate covariance; i.e., an appropriate time constant

value. Regarding the **GPS** measurements, as an example of the trade-offs involved, trusting more (i.e., smaller scalar covariance) the **GRAPHIC** data than the **SDCP** data will yield a more accurate absolute navigation. This is because the **SDCP** measurements work as a rigid connection between both **S/Cs**; trusting more this measurements will give a better relative navigation but could produce an offset in the absolute navigation outputs.

The **EKF** tuning, of course, depends on the operating scenarios of the filter. Then, a unique set of parameters can't appropriately cope with all the operational phases.

(h) The accuracies expected from **PRISMA** mission for real-time navigation, considering errors as differences of the actual variables *w.r.t.* the ones obtained with the ground truth model, and computing statistics after the **EKF** convergence phase, are:

- **Open-loop (no maneuvers) navigation (nominal):**

- Absolute position:  $< 2$  m (3D RMS).
- Relative position:  $< 4$  mm (3D RMS).
- Relative velocity:  $\sim 6$   $\mu\text{m/s}$  (3D RMS).
- Empirical accelerations (due to unmodeled forces):  $< 100$   $\text{nm/s}^2$  (3D RMS).

- **Closed-loop (including maneuvers) navigation (nominal):**

- Absolute position:  $< 3$  m (3D RMS).
- Relative position:  $\sim 4$  mm (3D RMS).
- Relative velocity:  $\sim 10$   $\mu\text{m/s}$  (3D RMS).
- Empirical accelerations (due to unmodeled forces):  $< 10000$   $\text{nm/s}^2$  (3D RMS).

In the closed-loop scenario, there is a slight degradation of the relative navigation accuracy. The relative velocity along-track and cross-track components graphs (having maneuvers only applied on those directions) shows errors at the time instants of maneuver occurrence, then damped over time.

The deterministic feedback control law makes use of the input absolute orbit states (for both **S/C**) generated by the **GOP** at 1 Hz rate. The maneuver commands are fed to the propulsion system model and to the accelerometer model as previously described. Consequently, maneuver execution errors are introduced in the numerical orbit propagation, and realistic accelerometers measurements are provided to the navigation filter for the incorporation of maneuvers.

Anyway, the orbit propagation accuracy is worse in closed-loop than in open-loop. Before the **EKF** could provide an update, we have only **GOP** extrapolating/updating the polynomials; we have a relation between maneuver knowledge error and navigation error. Additionally, **GOD** system makes only one measurement update (out of a total of 36 measurements) at a time (scalar update of the **EKF**). This makes very hard for this scheme to absorb the effect of a maneuver.

## 7 Acronyms

<b>AOCS</b>	Attitude and Orbit Control Subsystem
<b>ATO</b>	Along-Track Orbit
<b>CM</b>	Center of Mass
<b>CoNAE</b>	Comisión Nacional de Actividades Espaciales
<b>CRD</b>	Cartesian, Rectangular and Dextral
<b>DCM</b>	Direction Cosine Matrix
<b>DDCP</b>	Double-Difference Carrier Phase
<b>d.e.</b>	differential equation
<b>DEM</b>	Digital Elevation Model
<b>DLR</b>	<i>Deutsches Zentrum für Luft- und Raumfahrt</i> (German Aerospace Center)
<b>DSS</b>	Distributed Space Systems
<b>ECEF</b>	Earth-Centered, Earth-Fixed (reference frame)
<b>ECI</b>	Earth-Centered Inertial (reference frame)
<b>ESA</b>	European Space Agency
<b>FDIR</b>	Fault Detection, Isolation and Recovery
<b>FF</b>	Formation Flying
<b>FPGA</b>	Field-Programmable Gate Array
<b>GCO</b>	General Circular Orbit
<b>GEO</b>	Geostationary Earth Orbit
<b>GNSS</b>	Global Navigation Satellite System
<b>GOD</b>	GPS-based Orbit Determination
<b>GOP</b>	GPS-based Orbit Prediction
<b>GPS</b>	Global Positioning System
<b>GRAPHIC</b>	GRoup And PHase Ionospheric Correction
<b>GVE</b>	Gauss' Variational Equations
<b>HCW</b>	Hill-Clohessy-Wiltshire
<b>HEO</b>	High Earth Orbit
<b>HIL</b>	Hardware In-the-Loop
<b>ITO</b>	In-Track Orbit
<b>KF</b>	Kalman Filter
<b>EKF</b>	Extended Kalman Filter
<b>UKF</b>	Unscented Kalman Filter
<b>LEO</b>	Low Earth Orbit
<b>LISA</b>	Laser Interferometer Space Antenna
<b>LPE</b>	Lagrange's Planetary Equations
<b>LQR</b>	Linear Quadratic Regulator

<b>LTV</b>	Linear Time-Varying
<b>LVLH</b>	Local-Vertical, Local- Horizontal
<b>MPC</b>	Model Predictive Control
<b>MSE</b>	Mean Square Error
<b>NASA</b>	National Aeronautics and Space Administration (USA)
<b>NWO</b>	New Worlds Observer
<b>OE</b>	Orbital Elements
<b>OED</b>	Orbital Elements Differences
<b>PCO</b>	Projected Circular Orbit
<b>PRISMA</b>	Prototype Research Instruments and Space Mission tech. Advancement
<b>RF</b>	Radio-Frequency signals
<b>RMS</b>	Root Mean Square
<b>ROE</b>	Relative Orbital Elements
<b>S/C</b>	spacecraft
<b>SAR</b>	Synthetic Aperture Radar
<b>SDCP</b>	Single-Difference Carrier Phase
<b>SDPR</b>	Single-Difference Pseudo-Range
<b>SNR</b>	Signal-to-Noise Ratio
<b>SoC</b>	System-on-Chip
<b>STM</b>	State Transition Matrix
<b>SV</b>	Space Vehicle
<b>TAFF</b>	TanDEM-X Autonomous Formation Flying experiment
<b>TH</b>	Tschauner-Hempel
<b>VOP</b>	variation-of-parameters
<b>w.r.t.</b>	with respect to
<b>WC</b>	worst-case
<b>YA</b>	Yamanaka-Ankersen